UNIVERSIDAD SAN FRANCISCO DE QUITO USFQ

Colegio de Posgrados

Study of shock waves propagation by optical sensing using optical feedback interferometry

Tesis en torno a una hipótesis o problema de investigación y su contrastación

David Andrés Rivadeneira Bolaños

Julien Perchoux, PhD
Director de Trabajo de Titulación

Trabajo de titulación de posgrado presentado como requisito
para la obtención del título de Magíster en Nanoelectrónica

Quito, enero 2023

UNIVERSIDAD SAN FRANCISCO DE QUITO USFQ

COLEGIO DE POSGRADOS

HOJA DE APROBACIÓN DE TRABAJO DE TITULACIÓN

Study of shock waves propagation by optical sensing using optical feedback interferometry

David Andrés Rivadeneira Bolaños

Nombre del Director del Programa:	Luis Miguel Prócel
Título académico:	Doctor of Philosophy
Director del programa de:	Maestría en Nanoelectrónica

Nombre del Decano del colegio Académico:	Eduardo Alba
Título académico:	Doctor of Philosophy
Decano del Colegio:	Colegio de Ciencias e Ingenierías

Nombre del Decano del Colegio de Posgrados:	Hugo Burgos
Título académico:	Doctor of Philosophy

Quito, enero 2023

© DERECHOS DE AUTOR

ACLARACIÓN PARA PUBLICACIÓN

Nota: El presente trabajo, en su totalidad o cualquiera de sus partes, no debe ser considerado como una publicación, incluso a pesar de estar disponible sin restricciones a través de un repositorio institucional. Esta declaración se alinea con las prácticas y recomendaciones presentadas por el Committee on Publication Ethics COPE descritas por Barbour et al. (2017) Discussion document on best practice for issues around theses publishing, disponible en http://bit.ly/COPETheses.

UNPUBLISHED DOCUMENT

Note: The following graduation project is available through Universidad San Francisco de Quito USFQ institutional repository. Nonetheless, this project – in whole or in part – should not be considered a publication. This statement follows the recommendations presented by the Committee on Publication Ethics COPE described by Barbour et al. (2017) Discussion document on best practice for issues around theses publishing available on http://bit.ly/COPETheses.

DEDICATORIA

Dedico el presente trabajo a mis padres Katia y Ramiro, cuyo invaluable soporte y apoyo incondicional fue la base y el motor para lograr terminar con éxito la maestría de Nanoelectrónica de la USFQ.

AGRADECIMIENTOS

Agradezco a mi tutor Julien Perchoux por guiarme en la realización del presente trabajo de investigación, por su retroalimentación durante este proyecto, y por sus consejos para la presentación de este ante al jurado de la universidad ENSEEIHT de Toulouse.

RESUMEN

Realicé mi pasantía de fin de estudios en las instalaciones de LAAS en la ENSEEIHT. El propósito de la pasantía fue la mejora del procesamiento de señales de auto-mezcla (SM) medidas por sensores de interferometría de retroalimentación óptica (OFI) para medir los cambios de presión producidos por ondas de choque. En este trabajo se consideraron varios métodos de procesamiento de señales, algunos de los cuales involucraron ondículas y un filtro de paso bajo. La mejora propuesta más importante fue la modificación del algoritmo utilizado para calcular una derivada en el algoritmo de un pasante anterior que trabajaba en este proyecto. Esto proporciona una mejora en la determinación de la dirección de las franjas. Sin embargo, no fue posible lograr una detección automática de las franjas de frecuencia rápida que son las franjas más importantes de la señal, a pesar de intentar una solución con ondículas.

Palabras clave: interferometría de retroalimentación óptica, onda de choque, franja, ondícula, explosión.

ABSTRACT

I realized my end-of-studies internship at the LAAS facilities at ENSEEIHT. The purpose of the internship was the improvement of the signal processing of self-mixing (SM) signals measured by optical feedback interferometry (OFI) sensors to measure the pressure changes produced by shock waves. Several signal processing methods were considered in this work, some of which involved wavelets, and a low pass filter. The most important proposed improvement was the modification of the algorithm used to calculate a derivative in the algorithm of a previous intern working in this project. This provides an improvement in the direction determination of fringes. It was however not possible to achieve an automatic detection of the fast-frequency fringes that are the most important fringes in the signal, despite trying a solution with wavelets.

Key words: optical feedback interferometry, shock wave, fringe, wavelet, explosion.

TABLE OF CONTENTS

LIST OF TABLES

LIST OF FIGURES

INTRODUCTION

Presentation of the laboratory

The LAAS (Laboratoire d'analyse et d'architecture des systèmes), located in Toulouse, France, is a CNRS (Centre national de la recherche scientifque) research unit linked to the Institute for Engineering and Systems Science (INSIS) and the Institute of Information Sciences and their Interactions (INS2I).

The application domains of the laboratory are the following: aeronautics and space, telecommunications, transports, production, services, security and defense, energy management, healthcare, environment and sustainable development.

Scientific research is distributed into the following departments:

- Critical Information Processing

- Networks and Communications

- Robotics

- Decision and Optimization

- MicroNanosystems RF and Optics

- Nano-Engineering and Integration

- Energy Management

- MicroNanoBio Technologies

Context of the project

The project takes place in the OASIS group of the LAAS. The OASIS group is dedicated to the design of optical interferometric sensors and its associated electronics. Within the context of the Internet of Things (IoT), the group focuses on developing embedded and real-time

optoelectronic measurement devices. Research is done to explore the limits of the physics of the devices to reach state of the art performance of the developed sensors.

The project is done in collaboration with the "Commissariat à l'énergie atomique et aux énergies alternatives" (CEA), namely with the CEA center located in Gramat, France. The center is attached to the CEA's Military Applications Department, and is the defense reference center in terms of vulnerability of systems and infrastructures to the effects of weapons and effectiveness of conventional armaments. The main contribution to the project by this center was the access granted to its detonics laboratory, where the experiments involving the shock tube were performed.

The main objective of the project was to improve the signal processing algorithms proposed by previous interns, to use optical feedback interferometry (OFI) sensors to reconstruct the pressure as a function of time of a shock wave passing through the sensors. The signals measured by the OFI sensors must undergo a series of signal processing steps to reconstruct the shock wave pressure as a function of time. The shock wave is generated in a shock tube.

The state of the project before the internship began is the following. The first intern, Juan Jose Imas, performed the first shock tube experiments at the CEA center in Gramat. He developed also the first signal processing algorithms to reconstruct the shock wave pressure from the OFI signals. However, the algorithms needed further refinement to improve the pressure reconstruction.

The second intern in the project, Maiwenn Berthelot, developed a second signal processing algorithm that proved to be more robust than the one made by Imas. The processing was applied to some of the OFI signals measured by Imas. Her algorithm yielded an improvement in the detection of the main features of the OFI signal used to reconstruct the pressure. However, not all these features, called fringes, could be detected with the algorithm.

During my internship, I intended to provide further improvements in the signal processing algorithm used to reconstruct the pressure signal: it was desired to perfect the fringe detection. Furthermore, new measurements of OFI signals were performed during my internship, which were later processed by the algorithm I proposed.

Theory

The OFI sensor used in the CEA experiments can be modeled with a 3-mirror model explained in what follows. Figure 1 shows a schematic representation of a laser diode in an optical feedback interferometry set up. The laser is shown on the left, delimited by mirrors M1 and M2. The light output by the laser exits through mirror M2 into an external cavity, shown in the figure as the region between mirrors M2 and M3. The light is reflected by M3 (the reflecting target), and it is reinserted into the laser through M2. In the figure are shown the lengths of the laser cavity and the external cavity, L_{in} and L_{ext} respectively. The refractive indices of these regions are denoted as n_{in} and n_{ext}.
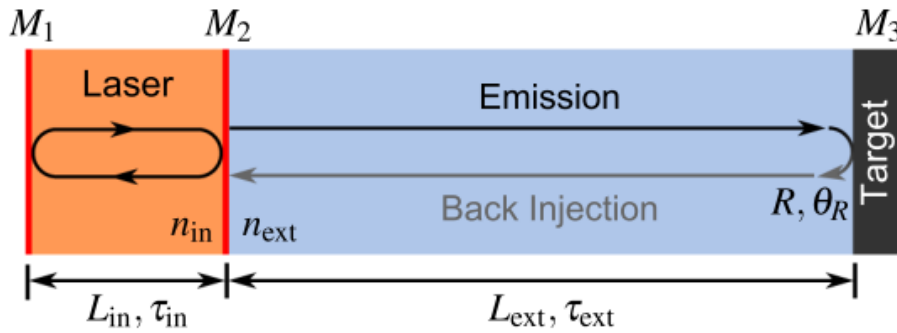
Figure 1 : Laser feedback interferometry 3-mirror model.

By considering that the OFI system has reached steady-state behavior, which happens when the frequencies of system stimuli are slow with respect to the natural frequencies of the system, the excess phase equation (Equation (1)) can be deduced.

$$\varphi_{FB} - \varphi_s + C \cdot \sin(\varphi_{FB} + \arctan(\alpha)) = 0 \qquad (1)$$

$$\varphi_s = \omega_s \tau_{ext}; \ \varphi_{FB} = \omega_{FB} \tau_{ext}$$

The parameters in Equation (1) are defined as follows (Taimre, et al., 2015):

α: linewidth enhancement factor.

C: feedback level/parameter. It affects the shape of the OFI signals.

τ_{ext}: external cavity round-trip time

ω_s: laser mode angular frequency in the absence of optical feedback.

ω_{FB}: laser mode angular frequency

φ_s: phase stimulus - the phase accumulated on transmission through the external cavity with the laser not undergoing optical feedback.

φ_{FB}: phase response - the actual phase accumulated on transmission through the external cavity.

The phase response φ_{FB} cannot be directly observed. However, the optical output power of the laser diode, P(t) can. This is given in equation (2) as a function of φ_{FB}, where P_0 is the output power when the laser undergoes no feedback.

$$P(t) = P_0\big[1 + m\cos\big(\varphi_{FB}(t)\big)\big] \tag{2}$$

A common application of OFI sensors is the measurement of the displacement of the target. The movement of the target results in a change in the length of the external cavity L_{ext}. This makes the phase stimulus φ_s vary according to equation (3).

$$\varphi_s(t) = \omega_s \tau_{ext} = \frac{2\pi c}{\lambda} \cdot \frac{2 n_{ext} L_{ext}(t)}{c} = \frac{4\pi n_{ext} L_{ext}(t)}{\lambda} \tag{3}$$

It should be noted that by changing the length L_{ext} by $\frac{\lambda}{2 n_{ext}}$, we get the same output power P that we have at the length L_{ext}. This can be explained as follows. If φ_s is viewed as a function of L_{ext}, then we have the following:

$$\varphi_s(L_{ext}) = \frac{2\pi c}{\lambda} \cdot \frac{2n_{ext}L_{ext}}{c} = \frac{4\pi n_{ext}L_{ext}}{\lambda} \tag{4}$$

If L_{ext} is changed by $L'_{ext} = L_{ext} + \frac{\lambda}{2n_{ext}}$ then $\varphi_s(L'_{ext}) = \varphi_s(L_{ext}) + 2\pi$. If we make the

following definitions: $\varphi_{s1} = \varphi_s(L_{ext})$ and $\varphi_{s2} = \varphi_s(L'_{ext})$, then we have that $\varphi_{s2} = \varphi_{s1} +$

2π. If the pair $(\varphi_{FB1}, \varphi_{s1})$ is a solution to the excess phase equation, then it can be easily seen

that the pair $(\varphi_{FB2}, \varphi_{s2})$ is also a solution, where $\varphi_{FB2} = \varphi_{FB1} + 2\pi$. If we replace φ_{FB2} in the

optical output power equation, we get $P(\varphi_{FB2}) = P_0[1 + m\cos(\varphi_{FB2})] = P_0[1 +$

$m\cos(\varphi_{FB1} + 2\pi)] = P_0[1 + m\cos(\varphi_{FB1})] = P(\varphi_{FB1})$. In conclusion, for both lengths L_{ext}

and L'_{ext} we get the same output power $P(\varphi_{FB1})$.

Figure 2 shows in detail the set-up of an OFI sensor used to measure the pressure variations of

a sound source. The source can also be considered to be the braking membrane leading to a

shock wave in a shock tube. In this case, the external cavity length L_{ext} remains constant, and

it is rather the refractive index in the laser path that changes as a result of the pressure change.

In what follows, a change in refractive index Δn is related to the number of fringes it produces

in the SM signal. The refractive index can be a function of other parameters other than pressure.

As an example, Ciddor proposed a model in which the refractive index of air depends on the

laser wavelength, the temperature, the pressure, the relative humidity, and the CO_2 content

(Imas, 2019). This model, however, applies to a range of pressures of $0.1 - 1.4$ bar, and in the

present work, pressures above 5 bar were considered. This shows, nonetheless, that the

refractive index depends on other parameters besides pressure. However, in the following

derivation, only the dependence on pressure will be considered since no data was available on

other thermodynamic parameters for the experiments performed.
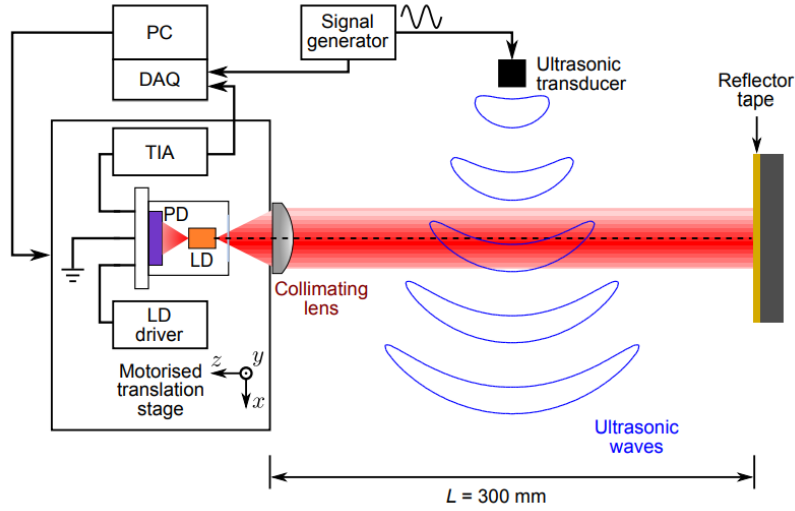
Figure 2 : Schematic representation of the OFI sensor for measurement of pressure inside shock tube. Taken from (Bertling, et al., 2014).

By replacing the definition of the phase response φ_{FB} given in equation (1) into equation (2), equation (5) is obtained.

$$P(t) = P_0[1 + m\cos(\omega_{FB}\tau_{ext})] \qquad (5)$$

The round-trip time of the laser in the external cavity τ_{ext} can be separated into two terms: τ_0, the round-trip time calculated for the constant refractive index n_0 along the length of the external cavity; and $\delta\tau$, the round-trip time corresponding to variations in the refractive index $\delta n(x)$ along the cavity length. This is expressed mathematically by equations (6) and (**7**), where the direction x is along the external cavity.

$$\tau_{ext} = \tau_0 + \delta\tau \qquad (6)$$

$$\tau_0 = \frac{2n_0 L_{ext}}{c} ; \delta\tau = \int_0^{L_{ext}} \frac{2\delta n(x)}{c} dx \qquad (7)$$

By assuming plane waves propagating perpendicularly to the external cavity, the dependence of $\delta n(x)$ on x is removed, as shown in equation (8), where Δn and therefore n' are constant along the external cavity.

$$\delta\tau = \frac{2\Delta n \cdot L_{ext}}{c} = \frac{2(n' - n_0)L_{ext}}{c} \tag{8}$$

By expressing the phase stimulus φ_s as a function of τ_0 and $\delta\tau$ we have equations (9) and (10), where the term φ_{s0} corresponds to n_0 and $\delta\varphi_s$ to the change in refractive index Δn.

$$\varphi_s(t) = \omega_s\tau_{ext} = \omega_s(\tau_0 + \delta\tau) = \frac{2\pi c}{\lambda}\left(\frac{2n_0 L_{ext}}{c} + \frac{2(n'(t) - n_0)L_{ext}}{c}\right) \tag{9}$$

$$\varphi_s(t) = \varphi_{s0} + \delta\varphi_s = \frac{4\pi n_0 L_{ext}}{\lambda} + \frac{4\pi(n'(t) - n_0)L_{ext}}{\lambda} \tag{10}$$

Finally, the number of fringes produced by the change Δn can be found using equation (11) below.

$$Number\ of\ fringes = \frac{\delta\varphi_s}{2\pi} = \frac{2\Delta n \cdot L_{ext}}{\lambda} \tag{11}$$

LITERATURE REVIEW

For the present work, the types of references consulted were the following: the reports of previous interns working on the project were consulted, also, peer review papers were used, finally, books on the topic were consulted. Concerning the structure used to organize the information, to begin, the previous intern reports were consulted as well as papers suggested by my tutor. Then, the cited references of these works were consulted as well as newer works citing the papers. Next, a keywords search was conducted on research-dedicated search engines. Finally, concerning the literature review design, the more recently published papers were considered as more important than older works.

METHODOLOGY AND DESIGN OF RESEARCH

Measurements

CEA measurements.

At the CEA facilities, shock waves were produced in a shock tube. Two experiment set-ups were used to measure the self-mixing signal variations produced by the passing of the shock wave at different points along the tube. Henceforth these set-ups will be referred to as the windows set-up and the arrow set-up. These will be described next.

In the windows set-up, three laser diodes were used, referred to as sensors 1, 3 and 4. The light coming from these sensors enters and exits the shock tube transversely through transparent windows, hence the name windows set-up. The positions of these sensors with respect to the shock tube are shown in Figure 3 and Figure 4. All three sensors were positioned near the end of the tube. For sensors 1 and 3, the reflecting target was the plate on which the other sensor was mounted on. Furthermore, a neutral density filter was placed in the path of both these sensors. With regards to sensor 4, the reflective target was a polished surface located inside the tube. Three experiments were performed in the windows configuration, these will be referred to as experiments 1 through 3.
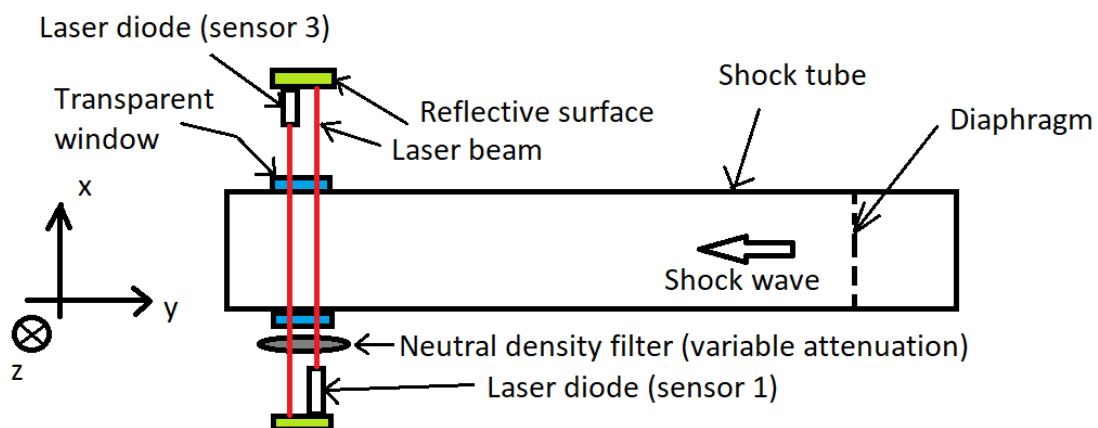
Figure 3: Windows set-up showing sensors 1 and 3
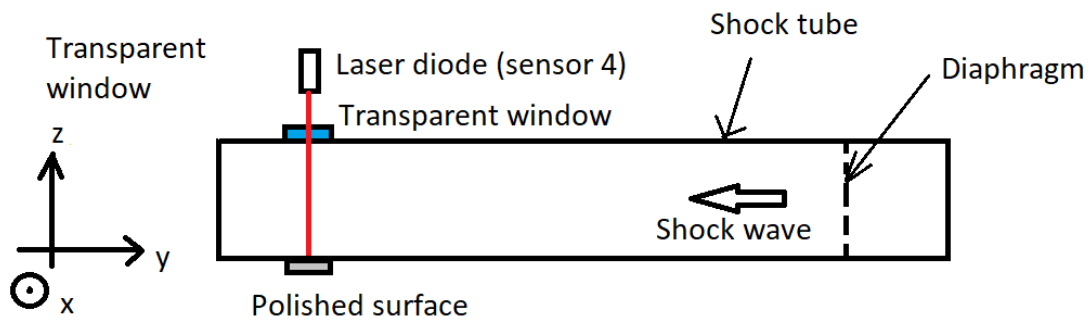
Figure 4: Windows set-up showing sensor 4

For the arrow experiment, the set-up was the one shown in Figure 5. In this case, two arrows were fixed at the end or the shock tube opposite to the breaking membrane. One arrow belongs to the CEA and contains pressure sensors. The other arrow belongs to the LAAS and contains a laser diode. Four experiments were performed in the arrow configuration. These are referred to as experiments 4 through 7. In experiments 4 through 6, the reflective target was the inner surface of the shock tube, while in experiment 7 it was the surface of the CEA arrow. The difference lies on the length of the external cavity, denoted as d and D in the figure.
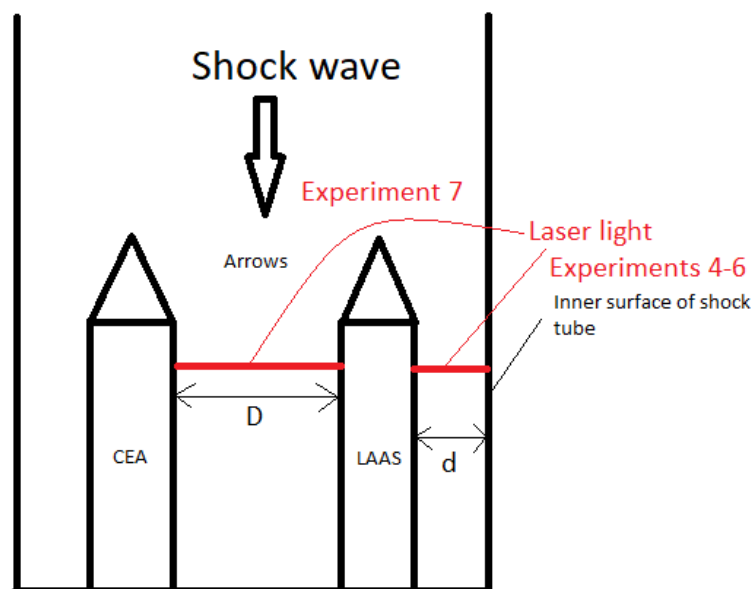
D: distance from laser's lens to CEA arrow's surface. D = 3 - 3.5 cm
d: distance from laser's lens to inner surface of shock tube. d = 2.5 cm

Figure 5 : Arrow experiments set-up. Target for experiments 4 – 6: inner surface of shock tube. For experiment 7: surface of CEA arrow.

In the appendix, at the end of this manuscript, the 7 experiments are detailed in the section "Annotations of the CEA experiments performed on July 1st 2021".

ENSEEIHT Measurements.

Some experiments were performed at the ENSEEIHT with the aim of discovering the best configuration of the optical feedback interferometry (OFI) sensor to be used in the CEA experiments so as to obtain measurements with the best signal-to-noise ratio, and fringes free of oscillations. An example of a fringe with oscillations is shown in Figure 6. The figure shows two fringes from a self-mixing (SM) signal measurement taken by an OFI sensor in a shock tube experiment at the CEA by a previous intern. The signal, labeled ref20, shows two fringes: the one on the left will be referred to as a clean fringe due to the clean jump discontinuity between samples $3.25 * 10^5$ and $3.3 * 10^5$. On the contrary, the fringe on the right does not have such a clean transition. In fact, there are several oscillations present at this transition. Such a fringe will be referred to as a dirty fringe or a fringe with oscillations.
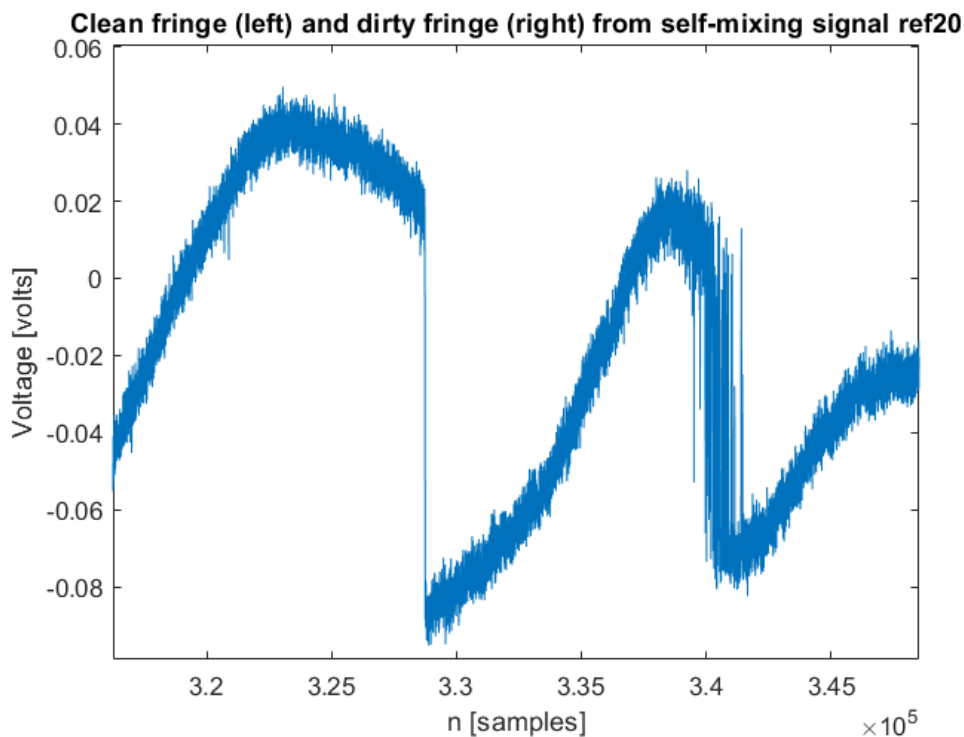
Figure 6 : Self-mixing signal with clean and dirty fringes.

Two types of experiments were performed at the ENSEEIHT: the speaker experiments and the ruler experiments. Each will be explained next.

Speaker experiments.

In this type of experiment, a laser diode directs its light towards a piece of reflective paper mounted on a vibrating speaker. The light impinges perpendicularly to the piece of paper, which vibrates back and forth at the fundamental frequency of the speaker, which can be regulated through an oscilloscope. The reflected light from the paper re-enters the laser creating a self-mixing signal. Sometimes an optical attenuator (Thorlabs part NDC-50S-1) was used in the experiments. A schematic diagram of the experiment configuration is shown in Figure 7.
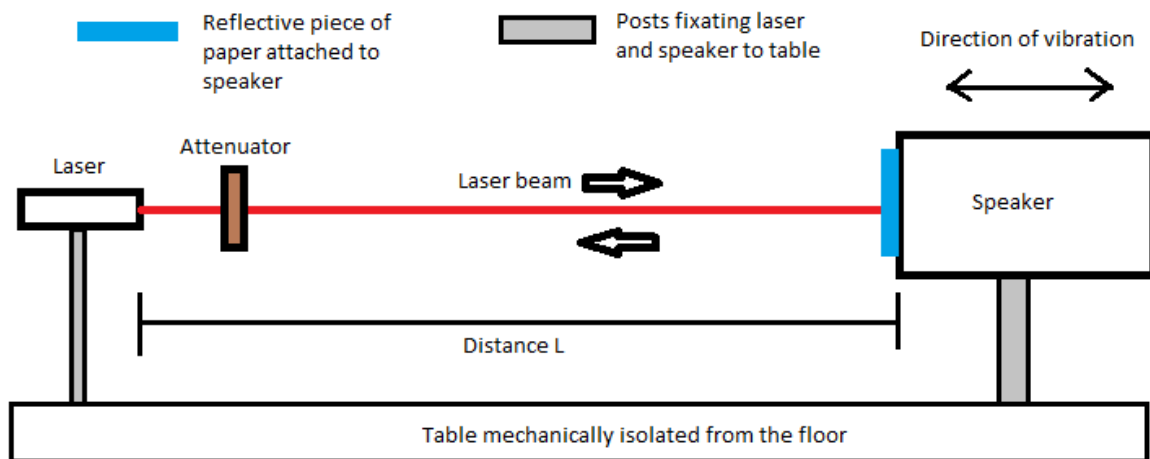
Figure 7 : Speaker experiment configuration

Two experiments, each varying two parameters, were made in this configuration. In each of them the distance from the laser to the speaker, shown as L in Figure 7, was varied. The distances used were 2, 5, 10, 20, and 40 cm, which are shown in Table 1 and Table 2 in the first column, preceded by a D, so D5 means a distance of 5 cm. The second variable was the attenuation of the neutral density filter, shown in Figure 7. Three values of attenuation were used, which correspond to the 3 strongest values of optical density. Also, the absence of attenuator was also considered. In experiment 1, the laser was collimated while in experiment 2, it was focused. For each pair of distance/attenuation used, either a Y or an N was assigned. Y means that dirty fringes such as that in Figure 1 were found in the SM signal acquired by the oscilloscope, while an N was assigned if none of these fringes were found. Table 1 and Table 2 show the results of experiments 1 and 2 respectively.

Table 1 : Results of experiment 1 (collimated beam). Optical density (OD) and external cavity length were varied.

	Collimated beam			
	Attenuation 1 (highest OD)	Attenuation 2 (2nd highest OD)	Attenuation 3 (3rd highest OD)	NA (No Attenuator)
D2	N	N	N	N
D5	N	N	N	N
D10	N	N	N	Y
D20	N	N	N	Y
D40	N	N	N	N

It must be said that for each pair of distance/attenuation in the tables, the laser was first turned off for 5 minutes to allow it to cool down, and then it was turned on for 3 minutes during which the visual judgement of whether or not dirty fringes were present was made. The switching off of the laser after 3 minutes was done to prevent the laser from reaching steady state, so during the 3 minutes of observation of the presence of fringes, the laser would go through different operating points. This was done because it was desired to see only the effect of varying the distance and the attenuation, so by having the laser operate in a transient mode, other parameters of the laser behavior would vary randomly during the three minutes, and this would allow to neglect their effect on the results given in Table 1 and Table 2.

Table 2 : Result of experiment 2 (focused beam). Optical density (OD) and external cavity length were varied.

	Focused beam			
	Attenuation 1 (highest OD)	Attenuation 2 (2nd highest OD)	Attenuation 3 (3rd highest OD)	NA (No Attenuator)
D2	Y	Y	Y	Y
D5	N	N	Y	Y
D10	N	Y	Y	Y
D20	N	N	Y	Y
D40	N	N	N	Y

By comparing the results in Table 1 and Table 2, it is seen that for the collimated laser experiment, the dirty fringes have only occurred for the No Attenuation (NA) case while for the focused beam experiment these fringes have occurred most often in the NA case and as the attenuation has become stronger, these fringes have occurred less and less frequently. Nonetheless, it should be noted that as the attenuation is increased, the SM signal recovered presents degradation in the signal to noise ratio, as can be seen qualitatively in Figure 8. The figure shows two SM signals: A1D2C (Attenuation 1, Distance 2 cm, Collimated laser), and A3D2C (Attenuation 3, Distance 2 cm, Collimated laser). It is seen that the more attenuated signal, A1D2C has a poorer signal to noise ration than the other signal, and the fringe jump discontinuity is not as sharp as in the other signal. This makes the signal processing of the SM signal more difficult. Finally, there is a tendency in Table 2 for dirty fringes to occur more frequently at shorter distances from the laser to the target. However, if the distance is increased indefinitely, the fringes in the SM signal cannot be easily identified. All in all, these two tables suggest that for the CEA experiments, a configuration with the laser collimated, a medium attenuation, and a medium distance would produce the best results.
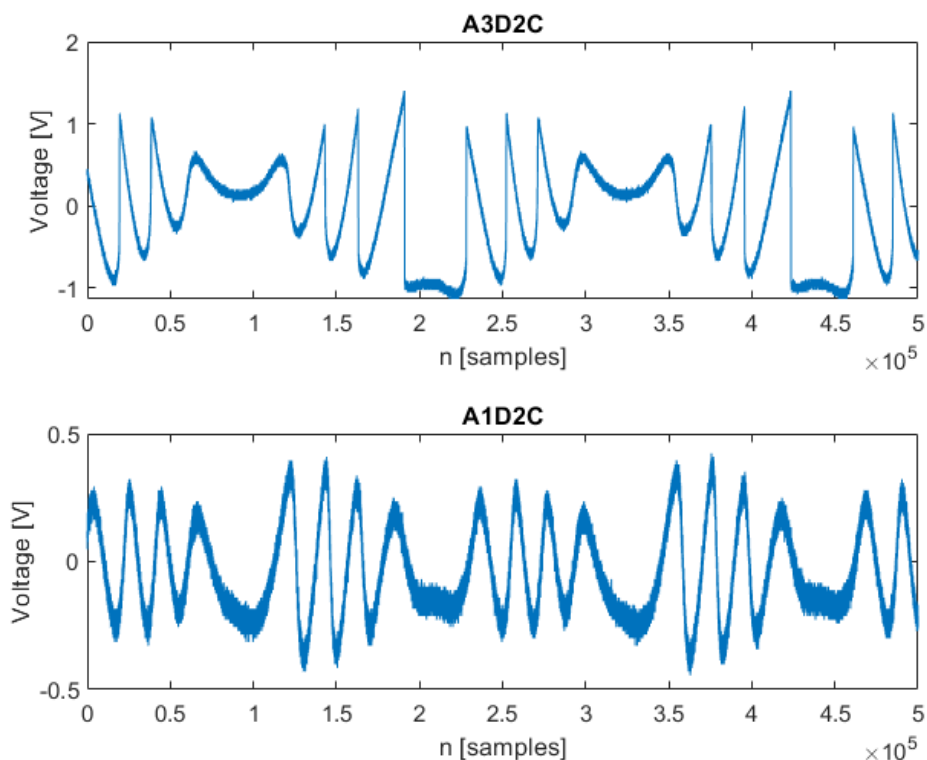
Figure 8 : Signals A3D2 and A1D2 from experiment 1 (Collimated). A stands for Attenuation (refer to Table 1). The more strongly attenuated signal presents a lower signal to noise ratio.

Ruler experiment.

In the speaker experiments, the speaker was driven by a sinusoidal signal generator. The frequency used to produce the results in Table 1 and Table 2 was 860 Hz. Since the target attached to the speaker vibrated at this frequency, and the frequency of the resulting fringes is related to the frequency of the moving target, the fringes produced were rather slow. In order to visualize fringes of a higher frequency, such as those seen in the CEA experiments, especially in the arrow configuration, it was necessary to increase the frequency of the speaker, however by doing so the speaker's diaphragm would vibrate with a smaller amplitude, and thus the amplitude of the fringes produced would have been too low to see, moreover, the speaker's sound became unpleasantly high at higher frequencies. Therefore, a new experiment using a metallic ruler was developed, which took the role of the vibrating target. The ruler's vibrations'

amplitude was visibly greater than that of the speaker's diaphragm, and good quality fringes were obtained as a result.

In the ruler experiment, a ruler was held in place at one end by a vise so as to have the ruler behave as a cantilever beam. The unconstrained end of the ruler was the laser's target. By giving the vise a slight hit with the finger, the ruler could vibrate. The length of the ruler that was not attached to the vise was set to be short enough that the fundamental frequency of the vibrating ruler, and thus the frequencies of the fringes in the SM signal, were higher than in the case of the speaker experiment. In this case, an attenuator was not included in the experiments, and a fixed distance D of around 3-5 cm was used between the laser and the ruler to simulate the external cavity in the case of the arrow experiments. A schematic of this experiment is shown in Figure 9.
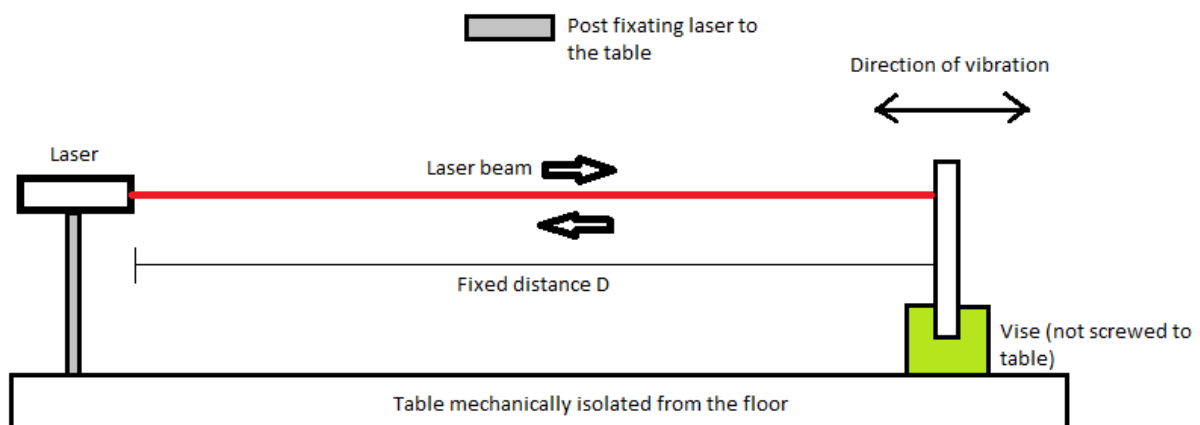
Figure 9 : Ruler experiment set-up

The conclusion of these experiments was that fringes with no oscillations were found with the laser collimated when white paper was the target. When the bare metallic surface of the ruler was the target, fringes with oscillations were found, with the laser collimated.

Signal Processing Methods Considered

Several signal processing options have been tried to improve the fringe detection capability of Maiwen's algorithm, to find a way to automatically detect regions where fringes have higher frequencies than in the rest of the signal, or to find simpler ways of processing the SM signals. Some of the results of these methods will be discussed in the section Results and Discussion. Next, these methods are explained.

Correlation with wavelets generated from a fringe pattern.

A problem in Maiwenn's algorithm is that it doesn't detect all the fringes present in the signal. One possible solution is to do a correlation between the self-mixing signal, and another signal having the shape of a fringe. This last signal could be for example a wavelet having the shape of a fringe. The cross-correlation is given by equation (12), where $x[n]$ is the SM signal as a function of the number of samples n, and ψ is in this case the wavelet.

$$(x \star \psi)[n] = \sum_{m=-\infty}^{\infty} \bar{x}[m]\psi[m+n] \tag{12}$$

Figure 10 shows two fringes extracted from signal ref20. The mean of each fringe has been removed in order to construct a wavelet from each fringe. A fast fringe and a slow fringe have been chosen so as to create a fast wavelet, and a slow wavelet, to be used to process the fast-fringe and slow-fringe regions. The removal of the mean is necessary for the wavelet construction because, by definition, a wavelet ψ must satisfy the following property:

$$\int_{-\infty}^{\infty} \psi(t)dt = 0 \tag{13}$$

So, considering that each fringe approximates a wavelet for the range of values of n shown in each plot in the figure, and that outside the range the wavelet is zero, by integrating each fringe over the n values shown in the plots after removing the mean, it's more likely to obtain a zero for the value of the integral, given the shape of the fringes. A value close to zero for this integral

shows that the fringe is a good candidate to be used as a pattern for building a wavelet. Figure 11 shows the wavelets generated from the fast and slow fringes using MATLAB's function `pat2cwav`.
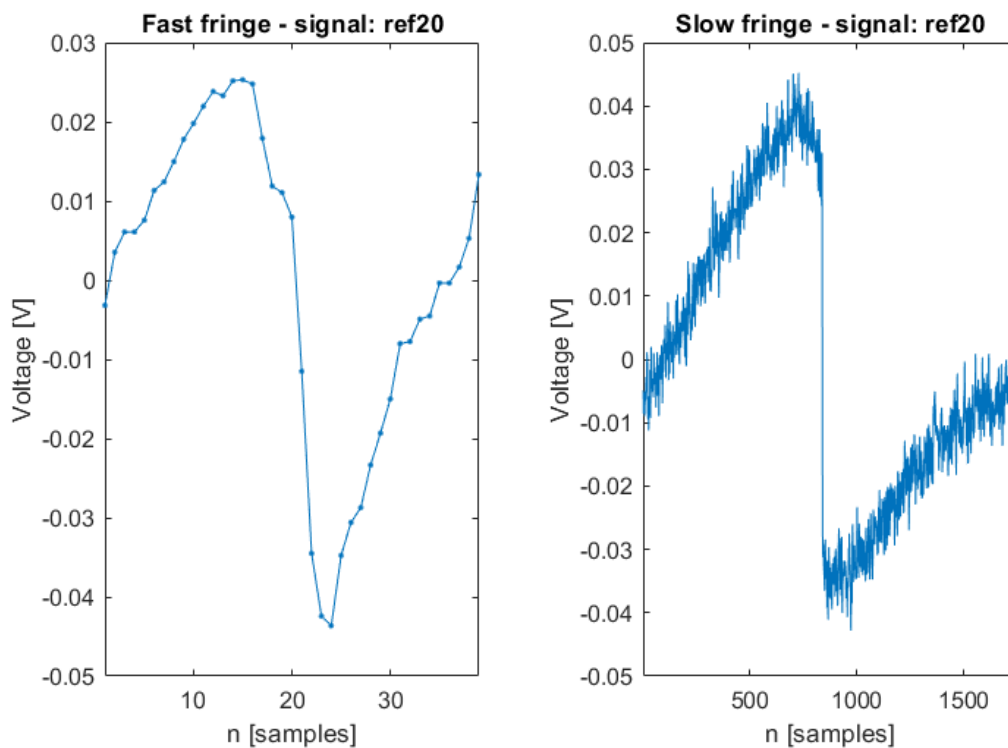
Figure 10 : Fast and slow fringes from signal ref20 to be used as models for wavelet construction.
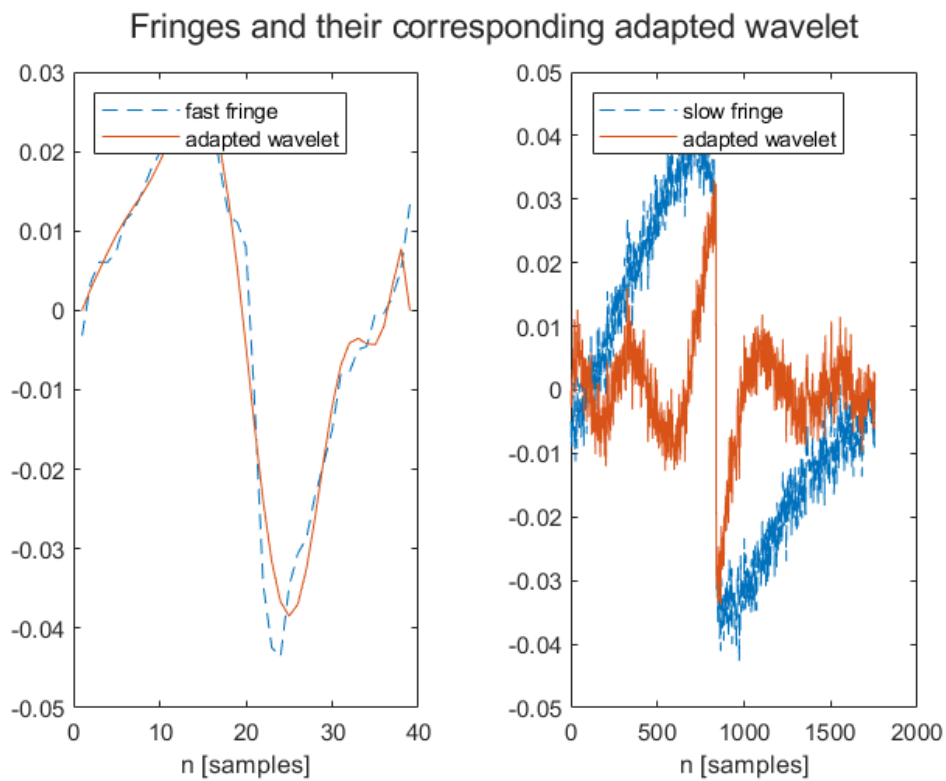
Figure 11 : Adapted wavelets generated from fast and slow fringes

Figure 12 below shows the comparison between the derivative of the signal used in Maiwenn's algorithm (see equation (14)), and the correlation of the SM signal with the fast and slow wavelets for the analysis of fast fringes. As the plot on the top shows, the slow wavelet is not able to detect the fringes present in the signal. However, the fast wavelet is able to detect the fringes. The detection is done using the findpeaks matlab function. With regards to the fringe detection capability, the performance of both maiwenn's derivative and the correlation with a fast wavelet is similar: The derivative detects just one more fringe.
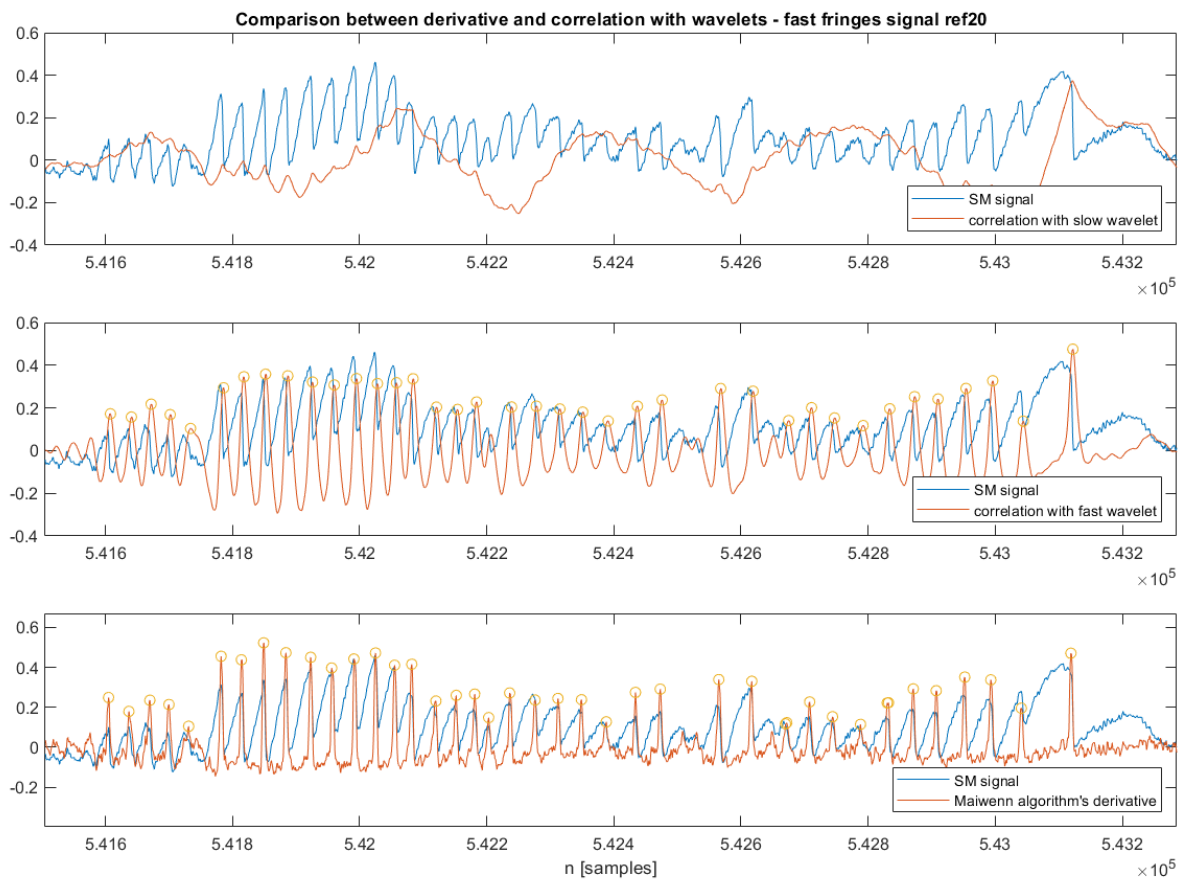
Figure 12 : Comparison between correlation with wavelets and application of derivative to detect fast fringes

Figure 13 shows the same as Figure 12, but for the slow fringes. In this case, both the correlation with the slow wavelet and the fast wavelet detect the fringes in the SM signal. An interesting thing to note is that the correlation with the slow wavelet near the fringes presents a waveform whose shape is not affected very much by the presence of oscillations in the fringes. For instance, for the second fringe from left to right, the shape of the waveform is similar to the shape of the waveform corresponding to the fringes on the left and on the right. This may be useful if it is not desired to detect the oscillations in one fringe as different fringes. The correlation with wavelets was not further explored since it was needed to better understand the theory behind wavelets to properly use them.
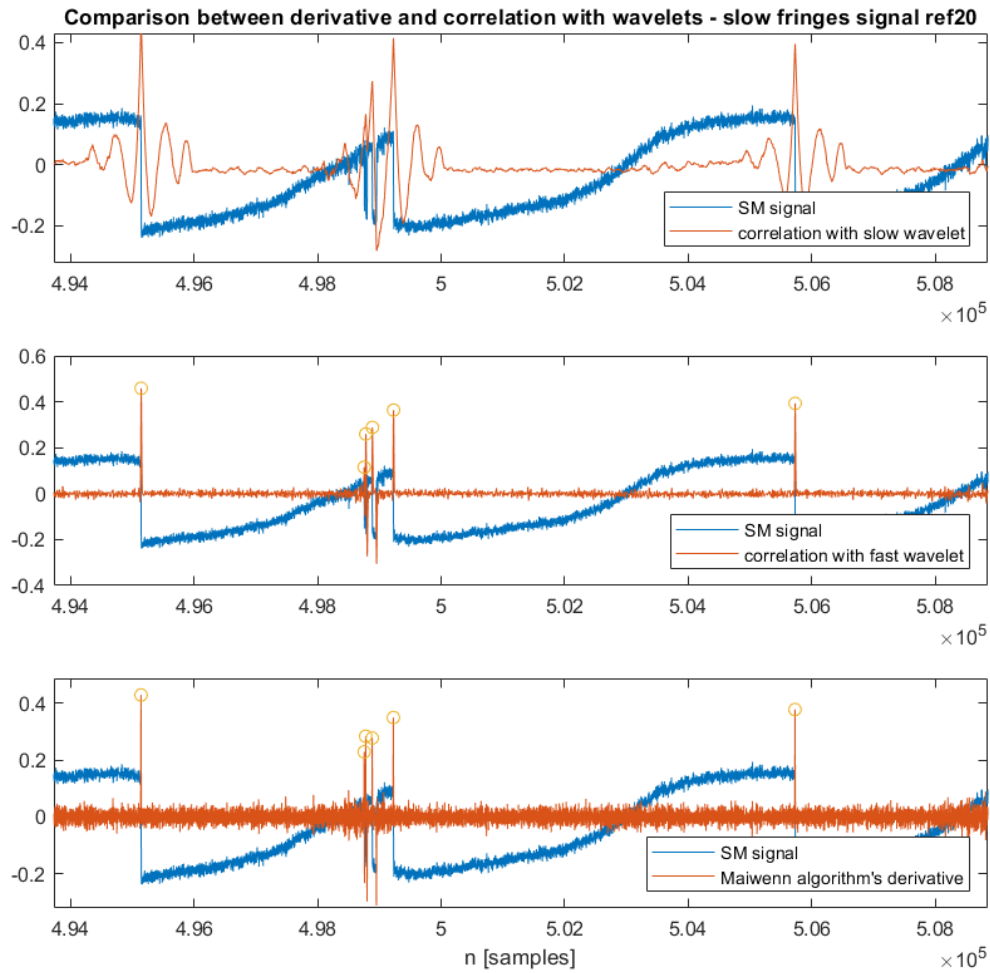
Figure 13 : Comparison between correlation with wavelets and application of derivative to detect slow fringes

Modification of Maiwenn's algorithm's derivative.

In Maiwenn's algorithm, particularly in the conditionment part of the self-mixing signal, the

derivative of this signal is approximated with equation (14), where x[n] is the self-mixing signal

as a function of the number of samples n.

$$x'[n] = \frac{x[n+5] - x[n]}{5} \qquad (14)$$

This approximation of the derivative is the average rate of change of x[n] with respect to n for

a 5-point interval. This interval width is rather large to produce a good enough approximation

of the derivative, and is problematic in Maiwenn's algorithm for detecting the jump

discontinuities in the fast fringes, which is a crucial step in detecting the fringes with said algorithm. This is illustrated in Figure 14, which shows a fast fringe from the self-mixing signal ref20, the approximation of its derivative in absolute value (henceforth referred to as the normalized derivative), the thresholded signal, and the 2 direction points obtained from the last signal by using Maiwenn's algorithm, which are used to determine the direction of the fringe, shown in the figure to be downward.
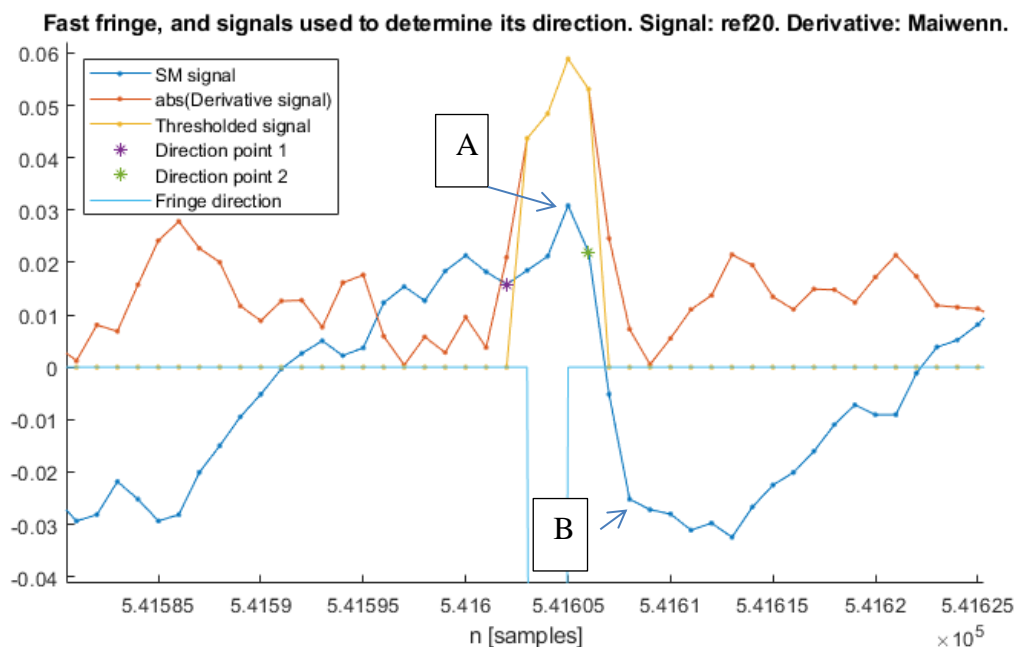
Figure 14 : Incorrect direction assignment to fast fringe using Maiwenn's 5-point derivative

The figure shows the normalized derivative; its maximum should ideally be located at a value of n somewhere between the start and the end of the fringe drop, which corresponds to the part of the SM signal between points A and B shown in the figure. Therefore, the normalized derivative approximation has a shift to the left in comparison to the signal it approximates, and so does the thresholded signal since it is calculated from the normalized derivative. This shift causes direction points 1 and 2 in the figure to also be shifted to the left. The green point should have an x coordinate slightly larger than point B, and the purple point should have an x coordinate slightly smaller to point A. So, for the fringe in the figure, the green point should

have a y value smaller than the purple point's. If that were the case, the fringe direction would be detected as going upward. However, since in the figure the green point is higher in the vertical axis than the purple point, the direction is incorrectly assigned as downward.

To fix the shift in time experienced by Maiwenn's 5-point derivative, it is possible to use a better approximation of the derivative which is no longer an average rate of change. It is proposed to use a discretization of the 5-point stencil derivative approximation (Sauer, 2012) given in equation (15) for a continuous function x(t) where t represents time.

$$x'(t) = \frac{-x(t + 2h) + 8x(t + h) - 8x(t - h) + x(t - 2h)}{12h} \qquad (15)$$

This formula calculates the derivative of x at t, using 4 other points: $t + 2h, t + h, t - h$, and $t - 2h$. This formula can be discretized by considering the following: $x[n] = x(nT_s)$ and $h = T_s$, where T_s is the sampling period of the self-mixing signal. So, we have the following discretized formula:

$$x'[n] = x'(nT_s)$$
$$= \frac{-x[n + 2] + 8x[n + 1] - 8x[n - 1] + x[n - 2]}{12h} \qquad (16)$$

Figure 15 below shows the same information as Figure 14 but using the 5-point derivative. As the figure shows, the derivative is not shifted to the left anymore, and this results in the correct placement of the direction points 1 and 2, delimiting the sharp drop in the fringe, which gives the correct fringe upward direction this time.
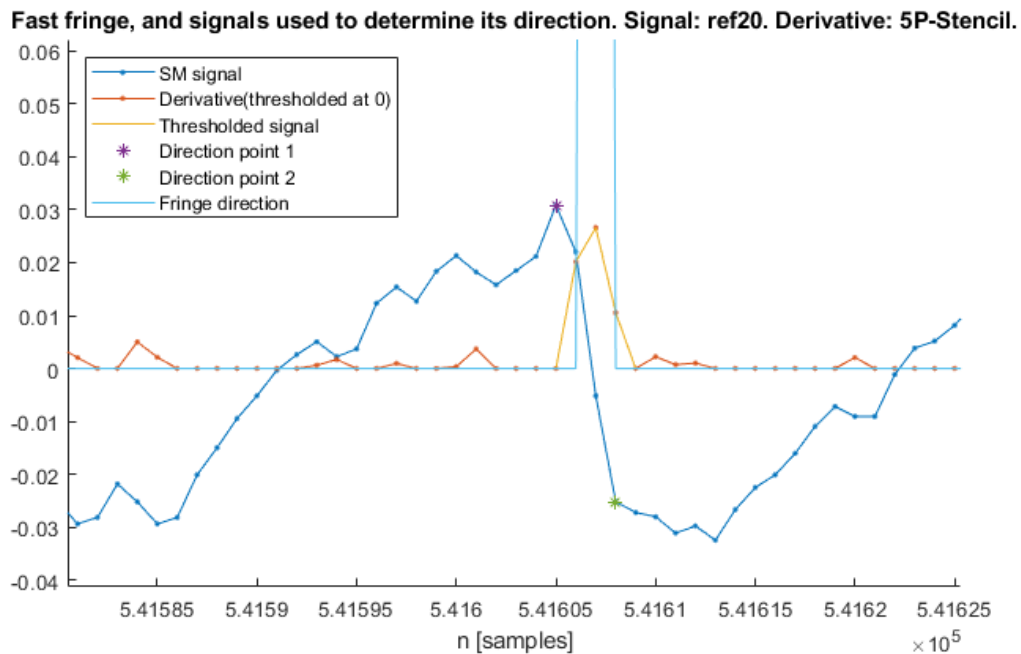
Figure 15 : Correct fringe direction assignment to fast fringe using 5-point stencil derivative

It is proposed to apply two algorithms to the SM signals and compare their performance. The first one is Maiwenn's algorithm, referred to as the MW algorithm; and the second one is Maiwenn's algorithm using the derivative in equation (16) rather than the one in equation (15). This modified algorithm will be referred to as the D algorithm. Before applying the two algorithms to the signals measured, it is necessary to explain the regions to be processed in the SM signal. The SM signal is associated to a pressure signal, so this signal will be explained first. Figure 16 below shows the pressure signal associated to the SM signal ref20. In the pressure signal, there are 6 regions that present a surge in pressure, which are labeled in the figure. To each of these regions corresponds a region in the associated self-mixing signal, characterized by fast fringes. For instance, in Figure 17, which shows part of the SM signal ref20, are shown the two fast-fringe regions corresponding to the rise 1 and rise 2 regions in Figure 16. The results of the comparison of the two algorithms will be shown in the section Results and Discussion.
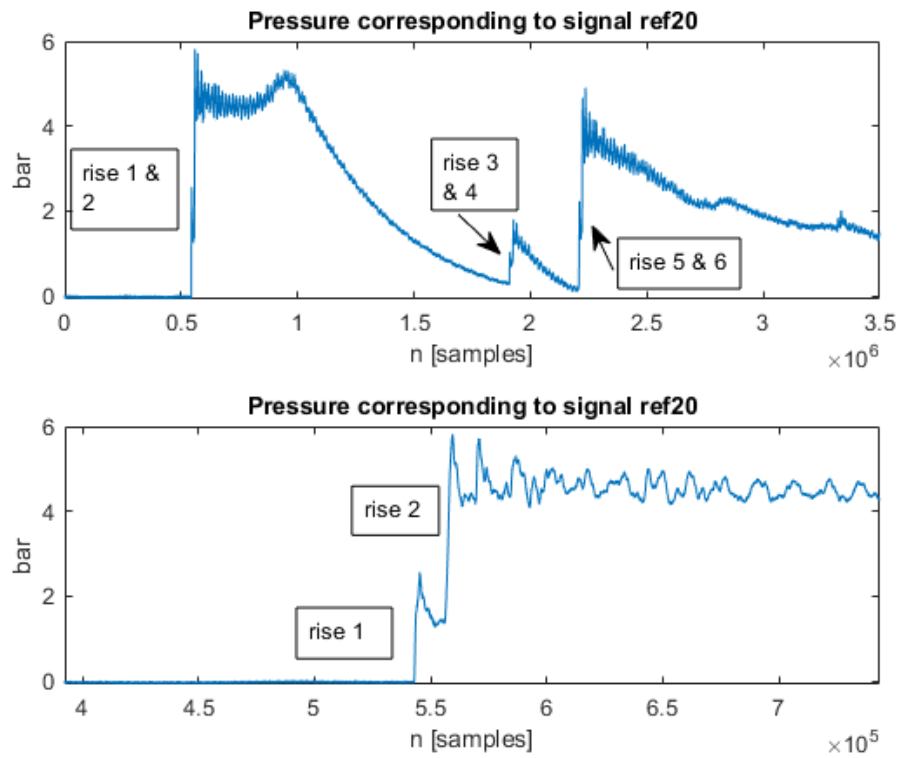
Figure 16 : Regions with a high increase in pressure. Fast fringes in the self-mixing signal are associated with them
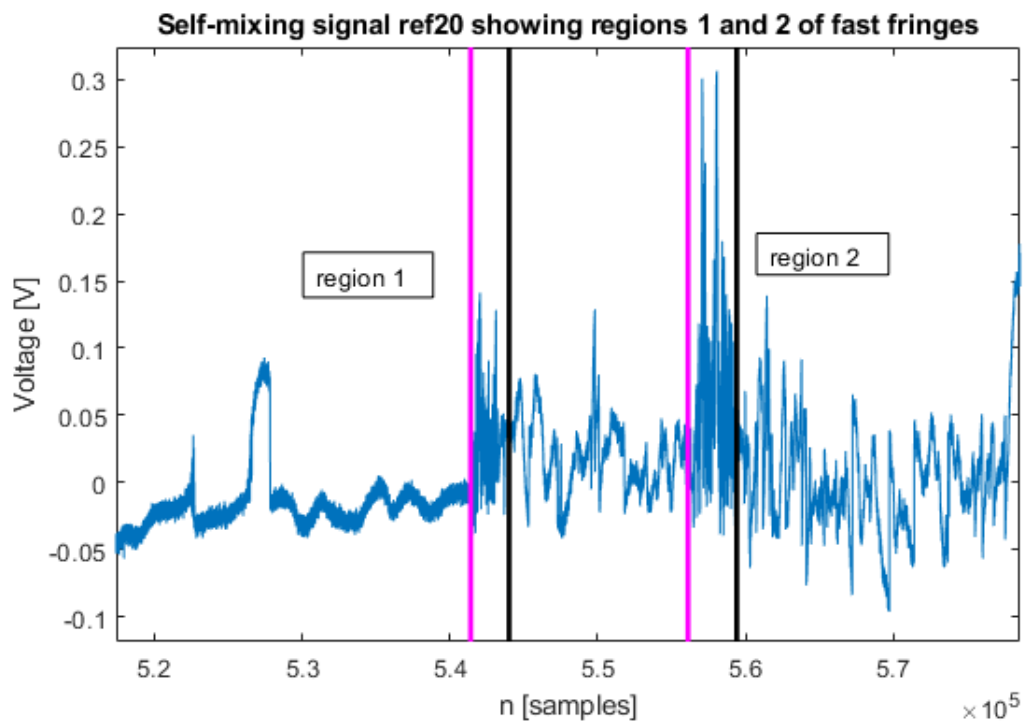

Figure 17 : Regions 1 and 2 of fast fringes, corresponding to regions rise 1 & 2 in Figure 16

Use of Continuous Wavelet Transform to detect start of fast fringes.

Wavelets could also be used with another purpose, namely, the detection of the start and end of

the fast-fringe zones in the SM signal, described in the preceding section. For this, the use of

the Continuous Wavelet Transform (CWT) is proposed. The definition of this transform is the

following:

$$C\big(a,b;f(t),\psi(t)\big) = \int_{-\infty}^{\infty} f(t)\frac{1}{a}\bar{\psi}\left(\frac{t-b}{a}\right)dt \tag{17}$$

The CWT basically compares the continuous-time signal $f(t)$ with compressed/stretched and

delayed versions of the wavelet $\psi(t)$. The parameter a in the above equation is the scale factor,

and it compresses or stretches the wavelet. The parameter b is the position factor, and it shifts

the wavelet along the time axis. Different wavelet functions can be chosen to apply the CWT,

depending on the features on the signal $f(t)$ that are being detected.

To apply the CWT in a computer, it is needed to discretize it. The discretization of the transform

that MATLAB uses is given in equation (18). In this expression, the continuous parameters t,

b, and a have been replaced by the discrete parameters n, m, and $2^{\frac{j}{v}}$. The parameters n, m, j,

and v are integers. MATLAB sets the parameter v, called the number of voices per octave, to

10 by default.

$$\frac{1}{a}\psi\left(\frac{t-b}{a}\right) \Longrightarrow \frac{1}{2^{\frac{j}{v}}}\psi\left(\frac{n-m}{2^{\frac{j}{v}}}\right) \tag{18}$$

The CWT was applied to signal ref20, particularly to the part of the signal shown in Figure 18,

which shows two fast regions of oscillation. The result, which is the spectrogram, can be seen

in Figure 19. It is noted here that the time axis in both figures was made to start at zero so that

the two plots could be compared.

Figure 19 shows three brackets, which correspond to the three brackets in Figure 18. The two red ones correspond to the fast fringes, and the green one corresponds to the slow fringes located between the two fast zones. By looking at the scalogram without looking at the SM signal in the time domain, it is not very clear which are the regions corresponding to fast fringes. For instance, the region indicated by the green bracket could be judged to be a region of fast fringes. For this reason, it was not possible to automatically detect the regions of fast fringes based on the scalogram. The problem being that the jump discontinuity in the slow fringes presents high-frequency components that are also found in the fast fringes, as the scalogram shows. This method was not explored any further since more knowledge about wavelets was required.
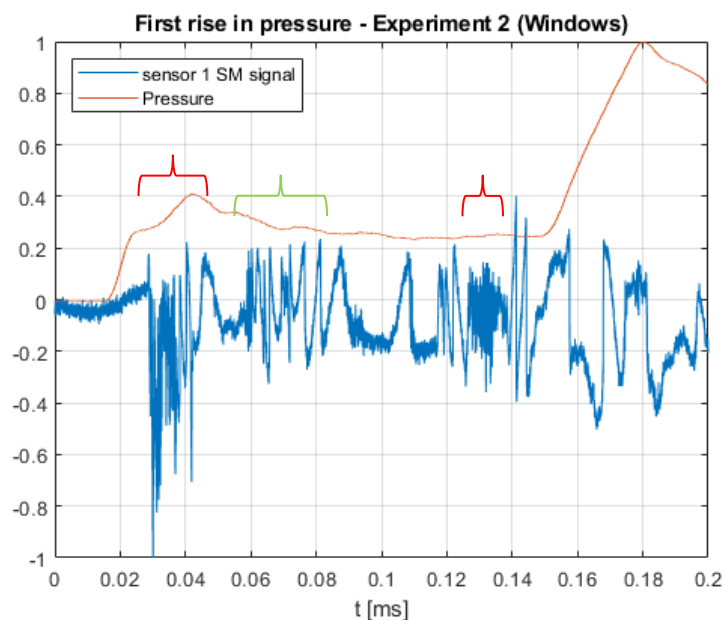
Figure 18 : SM signal ref20 with two regions of fast fringes, and pressure signal
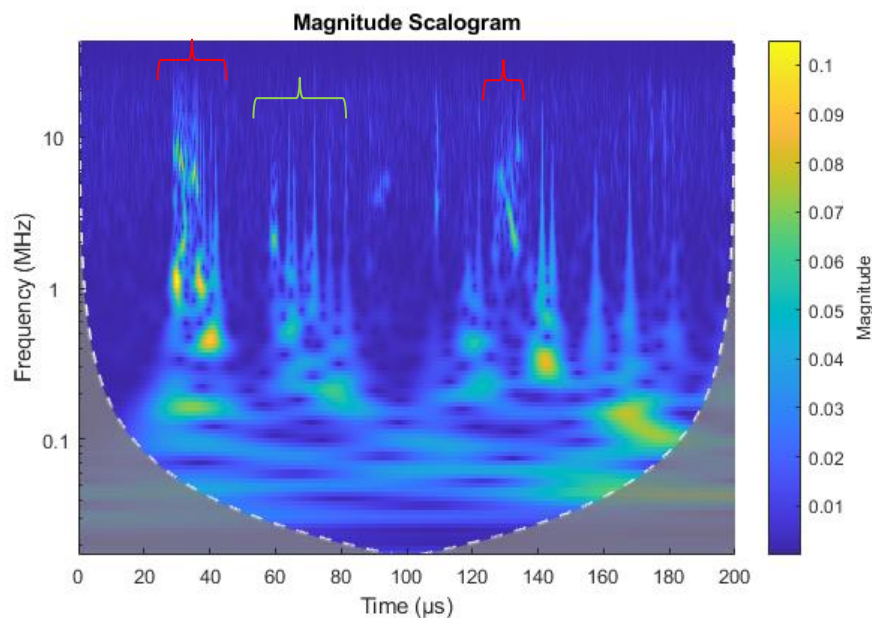
Figure 19 : Scalogram of SM signal shown in Figure 18

Application of a low pass filter to remove signal oscillations.

To remove the oscillations in the slow-oscillating fringes in the SM signal (see Figure 6), Maiwenn's algorithm does a convolution between the self-mixing signal and a Hamming window. In this operation, the window acts as a low-pass (LP) filter of the signal. However, a window doesn't provide the versatility of a dedicated filter, which by contrast, can be designed to have a specific cut-off frequency, and bandpass and bandstop frequencies. As an alternative to the windowing, or as a complement to it, it was proposed to design a LP FIR filter. A FIR filter is chosen because of its linear phase response in the bandpass region. This means that the time shift introduced in the signal is constant for all frequencies in the bandpass, so the signal is not distorted in the bandpass. Besides, the time-shift can be corrected easily. The results of the application of such a filter will be given in the next section.

DATA ANALYSIS

Modification of Maiwenn's algorithm's derivative

To measure the improvement provided by the 5-point stencil derivative on the signal processing, the MW and D algorithms were applied to two signals: ref20, and the signal from experiment 2 (window set-up, 5-bar), sensor 1 measured during this internship, henceforth referred to as the signal exp2-sen1. The signal processing was applied only on fast-fringe region 1, and the number of fringes and their directions in this region obtained with the two algorithms was recorded and compared to the actual number of fringes found (by counting by hand). Table 3 below summarizes the results for signal ref20.

Table 3 : Performance comparison results between Maiwenn's algorithm and modified Maiwenn's algorithm for signal ref20

Signal: ref20								
				Number of fringes				
Region	Before/After correction algorithms	Algorithm	Total (counted manually)	Total (counted by algorithm)	Correctly counted	Undetected	Incorrectly counted	Wrong direction
1	B	MW	42	38	36	6	2	2
		D		35	35	7	0	0
	A	MW		47	41	1	6	0
		D		46	39	3	7	0

In Table 3, the correction algorithms referenced in column 2 refer to the inverse fringe correction block and the missing fringe correction block in Maiwenn's algorithm (Berthelot, 2020). So, the two signal processing algorithms, MW and D, are compared in the table before (B) and after (A) applying both correction algorithms. The other columns in the table are explained next:

- Total counted by algorithm: Number of fringes automatically counted by the specified algorithm in the specified region of the SM signal.

- Correctly (or Incorrectly) counted: Fringes counted correctly by the algorithm. By referring to Figure 20, a correctly counted fringe is one for which the derivative of the SM signal is negative when the thresholded signal (conditionment block of Maiwenn's algorithm) is different than zero. The negative derivative corresponds to the sharp decrese in the fringe. On the other hand, if the derivative is positive, the fringe is considered to be incorrectly counted.

- Undetected: Number of fringes not detected by the algorithm; these fringes were counted by hand.

- Wrong direction: Number of fringes counted correctly, that is, with a downward direction assigned by the algorithm. Since the fast regions in the SM signal correspond to a rise in pressure, all these fringes must have the same direction, which is upward. The direction is determined by direction points 1 and 2 shown in Figure 15, which are generated by Maiwenn's algorithm.
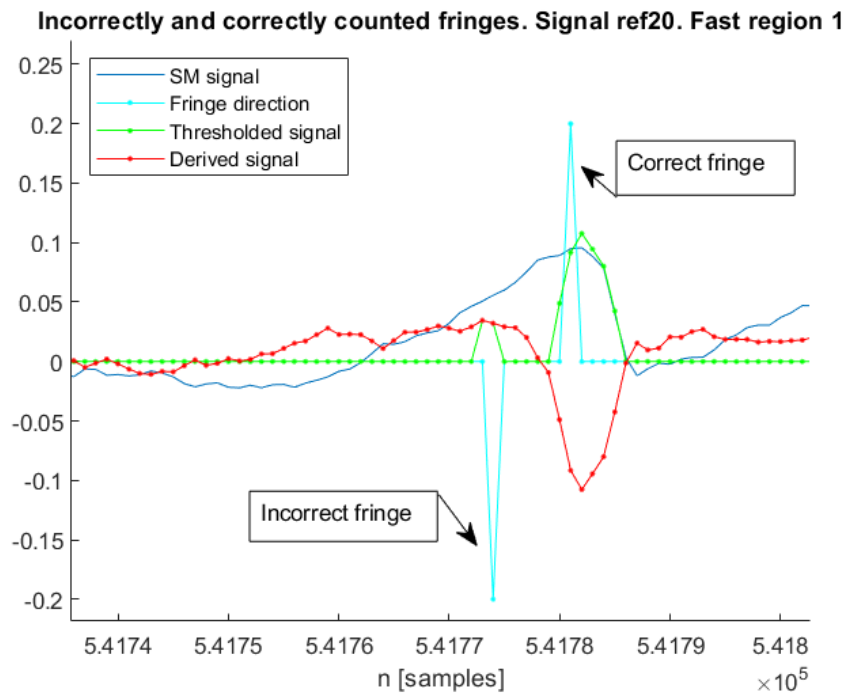
Figure 20 : SM signal showing an incorrectly and a correctly counted fringe.

By looking at Table 3, it is noted that before applying the correction algorithms, the MW algorithm finds 2 incorrect directions within the correctly counted fringes found, and counts 2 fringes incorrectly. On the other hand, the D algorithm does not assign any incorrect directions, nor does it count any incorrect fringes. In this aspect, the D algorithm performs better than the MW algorithm. This is shown by the highlighted cells in the table. On the other hand, the MW algorithm outperforms the D algorithm in the number of correctly counted, and undetected fringes, by one fringe in each case. All in all, the two algorithms have similar performance in this case.

With regards to the results after applying the correction algorithms, the following remarks are made. First, the number of fringes counted with the MW and D algorithms, 47 and 46 respectively, is larger than the actual number of fringes present (42). This causes the correctly counted fringes in both algorithms to approach better the actual number of fringes, but at the expense of having more incorrectly counted fringes for both algorithms. Second, for this region

and this signal in particular, the MW algorithm outperforms the D algorithm in the correctly, incorrectly, and undetected number of fringes, although the difference in performance is of at most 2 fringes in all 3 cases. Finally, the number of wrong directions is reduced to zero in both cases.

Table 4 shows the results for signal exp2-sen1 for region 1. In this case, it can be noted by the highlighted cells that the D algorithm outperforms the MW algorithm in every aspect. Before the correction algorithms no incorrect fringes are counted by the D algorithm, and the correctly counted fringes is 3 less than the actual number. After applying the correction algorithms, the number of correctly counted fringes equals the actual number, but at the expense of having 14 incorrect fringes. So in this case it is preferable to not apply the correction algorithms. For the MW algorithm, the application of the correction algorithms roughly doubles the number of incorrect fringes, and only increases in 1 the number of correct fringes. Moreover, both before and after the correction algorithms, the number of wrong directions detected is greater than 30, and the number of wrong directions is greater after the correction algorithms. On the contrary, the D algorithm finds no wrong fringe directions in any case.

Table 4 : Performance comparison results between Maiwenn's algorithm and modified Maiwenn's algorithm for signal exp2-sen1
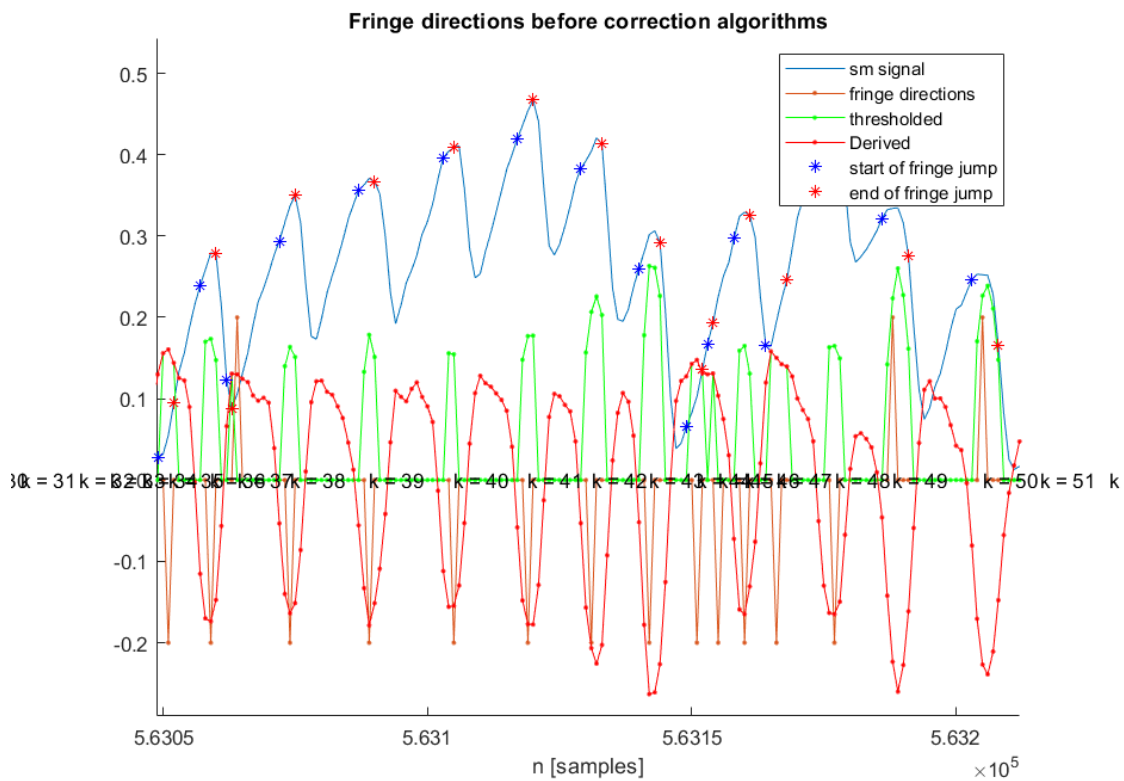
Signal: exp2-sen1								
			Number of fringes					
Region	Before/After correction algorithms	Algorithm	Total (counted manually)	Total (counted by algorithm)	Correctly counted	Undetected	Counted incorrectly	Wrong direction
1	B	MW	54	59	46	8	13	33
		D		51	51	4	0	0
	A	MW		71	47	8	24	37
		D		68	54	1	14	0

In summary, for the signal ref20 the MW algorithm outperforms the D algorithm in most cases, although the difference in performance for this signal in region 1 is not very important. On the other hand, for signal exp-sen1, the D algorithm outperforms the MW algorithm in every case, and the difference in performance is more noticeable this time. The fact that there is not one same algorithm that outperforms the other in both signals indicates that the thresholds used in both algorithms may well influence the results. However, these thresholds are at the present state assigned by hand, since no methodology to do the assignment based on some criteria has been found. A way to decide which algorithm performs better in general, is to process many fast-fringe regions, in the same manner in which they were processed in the two preceding tables. By processing many fast regions, the threshold assignment variable will not have an influence on the decision of which algorithm is better in general.

What is constant in the two previous tables, however, is that the D algorithm never assigns wrong directions to the fringes. Figure 21 shows the fringes detected by the D algorithm and their directions, which are correctly assigned as upward. Figure 22 shows the same as the previous figure but for the MW algorithm, and it shows incorrectly assigned downward directions for the fringes. Following the discussion for Figure 14 and Figure 15, the MW algorithm assigns the wrong direction because the points delimiting the start and end of fringe jump in Figure 22 are placed incorrectly due to the derivative used, which does not happen in Figure 21. Next, some of the signals measured at the CEA will be quickly analyzed to see the issues for their processing.
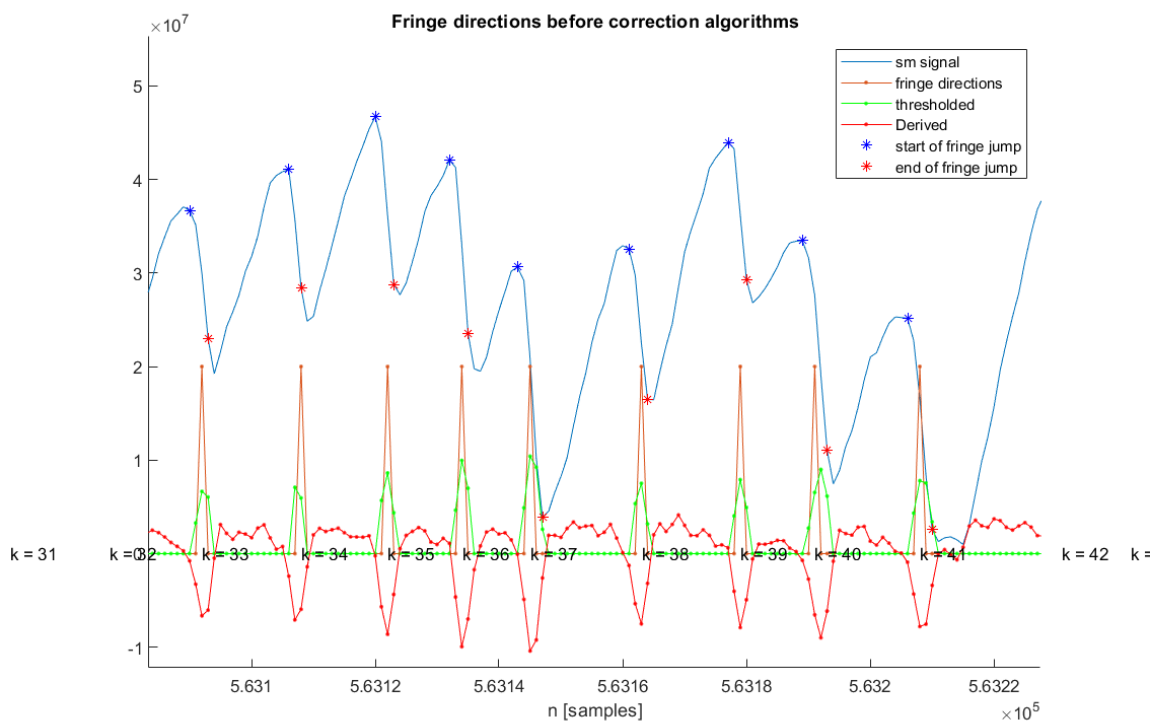

Figure 21 : Fringe directions using D algorithm for signal exp2-sen1

Figure 22 : Fringe directions using MW algorithm for signal exp2-sen1

Analysis of SM signal from experiment 3 (windows – 15bar)

Figure 23 shows a plot of the signal measured in experiment 3, sensor 4, henceforth referred to as exp3-sensor4, in part of region 1 of fast oscillations. This experiment corresponds to a 15-bar initial pressure in the shock tube. The blue curve represents the signal measured by the acquisition system and the red curve is the signal measured by the oscilloscope. It can be seen that there are fringes in the red signal that are not found in the blue signal. This indicates that the bandwidth of the acquisition system is not large enough to capture the fast fringes at the pressure of 15 bar. In the figure, the frequency of a fringe was measured to be around 24 Mhz. This means that the acquisition system should be modified so that signal components at this frequency are not attenuated. The figure also shows that the oscilloscope signal gets saturated at a little below -0.2 V. This should be fixed in future CEA experiments.
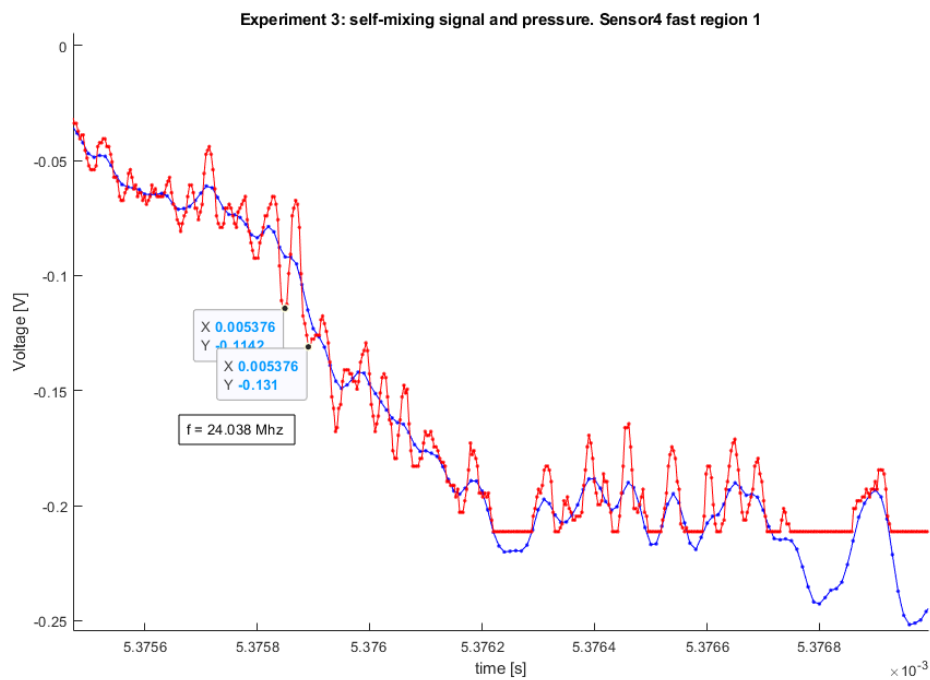
Figure 23 : Fringes of signal exp3-sensor4 (windows) in the region 1 of fast fringes.

**Analysis of SM signal from experiment 6 (arrow experiment)**

Figure 24 shows a plot of the SM signal from the acquisition system, and from the oscilloscope, for experiment 6 (15 bar), in which the OFI sensor in the arrow was used. The normalized pressure is also plotted. The figure shows a difference in the amplitudes of the oscilloscope signal and the acquisition system signal. This might be the result of an issue with an amplifier in the measurement systems. This should be checked for future measurements at the CEA facilities.
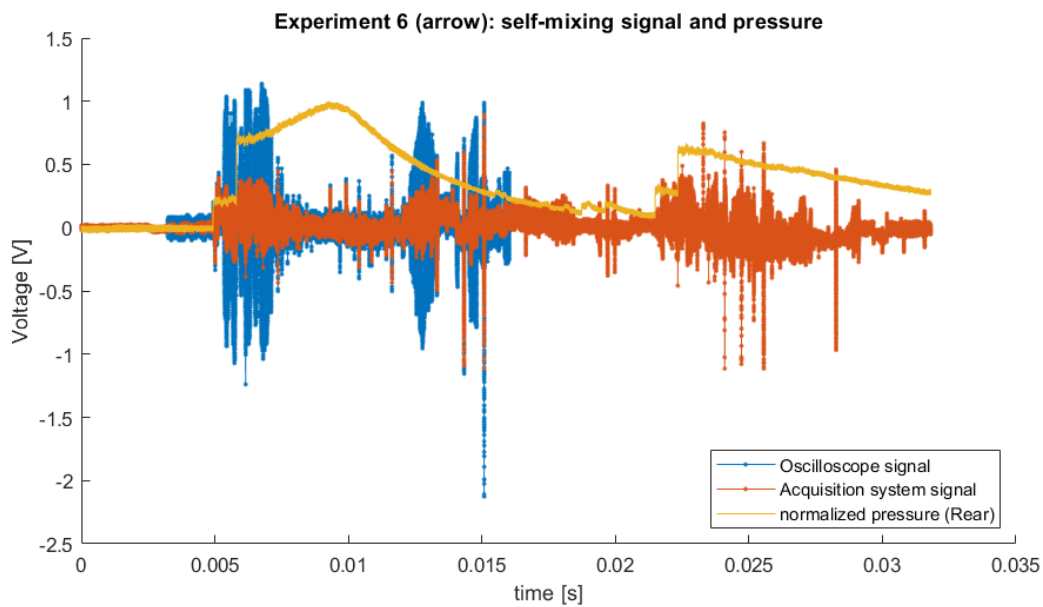
Figure 24 : Measurements for experiment 6 (arrow – 15 bar)

Figure 25 shows the same signals as Figure 24 at around 12 ms. The figure shows fringes poorly sampled by the acquisition system. The sampling is better for the oscilloscope signal but it is still not good enough since the fringe directions cannot be identified, even with the naked eye. The frequency of the fringes was estimated by measuring the period of a fringe, and this was obtained by placing two markers as shown in the figure. The frequency of the fringes is roughly 34.7 Mhz. At frequencies higher than 30 Mhz, the electronics in the OFI sensor attenuate the signals, so for future measurements in the CEA using the arrow configuration, the bandwidth of the sensor's electronics should be increased so as to be able to discriminate fringe directions. Finally, the application of a low-pass filter to an SM signal will be detailed next.
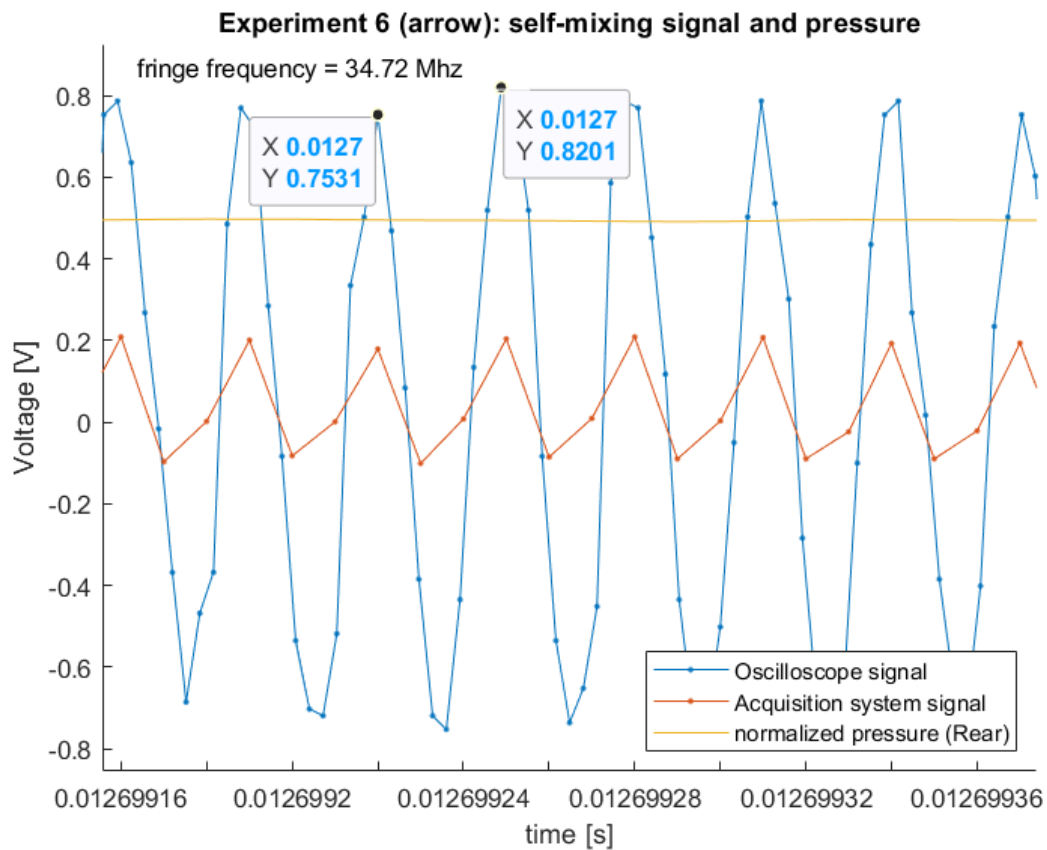
Figure 25 : Measurements for experiment 6 (arrow - 15 bar) - zoom

Application of a low pass filter to remove signal oscillations

A FIR filter was designed with the characteristics shown in Table 5 to process the slow fringes

in signal ref20.

Table 5 : Parameters for the design of the FIR filter

| Low-Pass FIR Filter parameter	Value
Bandpass frequency ω_p [$rad/sample$]	0.005π
Bandstop frequency ω_s [$rad/sample$]	0.007π
Stopband attenuation	$60\ dB$
Window	Blackman
Resulting filter order	5501

The bandpass frequency was selected by measuring the frequencies of the oscillations in fringes

such as the one in Figure 6, and choosing a frequency that was in the neighborhood by trial and

error. The bandstop frequency was chosen to be randomly close to the bandpass frequency. The

stopband attenuation was chosen randomly as 60 dB, and it was seen to be a good value after

filtering the SM signal. The blackman window was chosen since it can provide attenuation greater than 60 dB. Figure 26 shows the frequency response of the designed filter. In the figure, the phase plot shows the linear phase present in the bandpass region.
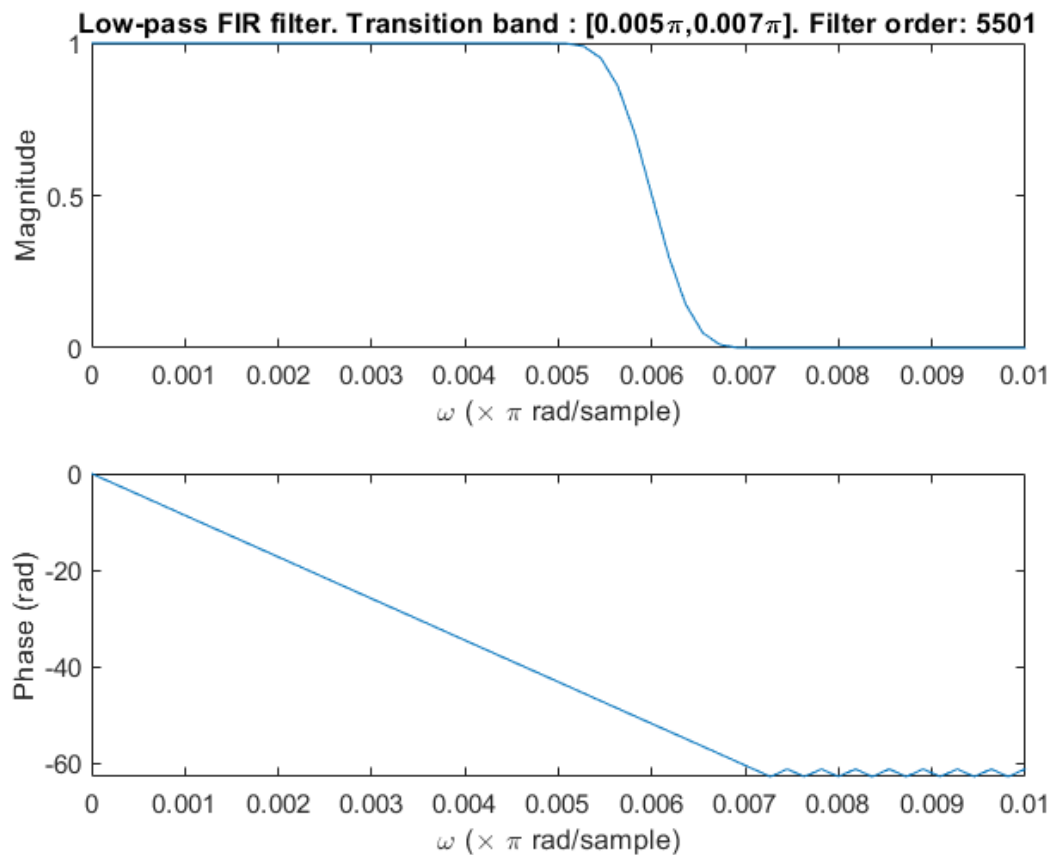

Figure 26 : Frequency response of designed FIR low-pass filter

By applying the filter to the SM signal ref20, Figure 27 through Figure 30 are obtained. Figure 27 shows the fringe in Figure 6 that has the oscillations, and the same fringe after filtering. As can be seen, the filtered fringe still has some oscillations that are then visible when taking the derivative of the filtered signal.
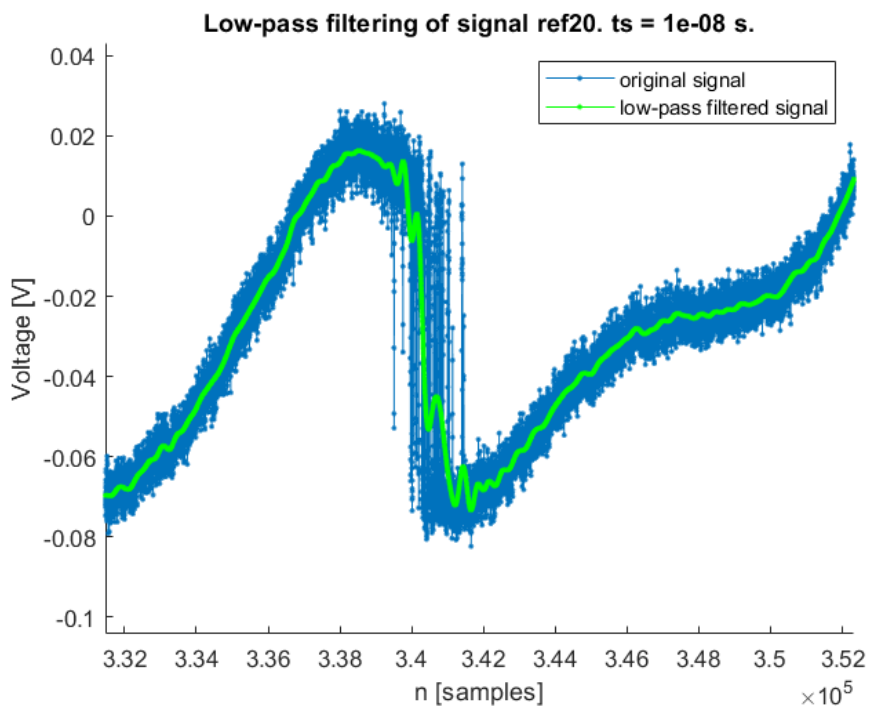
Figure 27 : Slow fringe with oscillations before and after low-pass filtering.
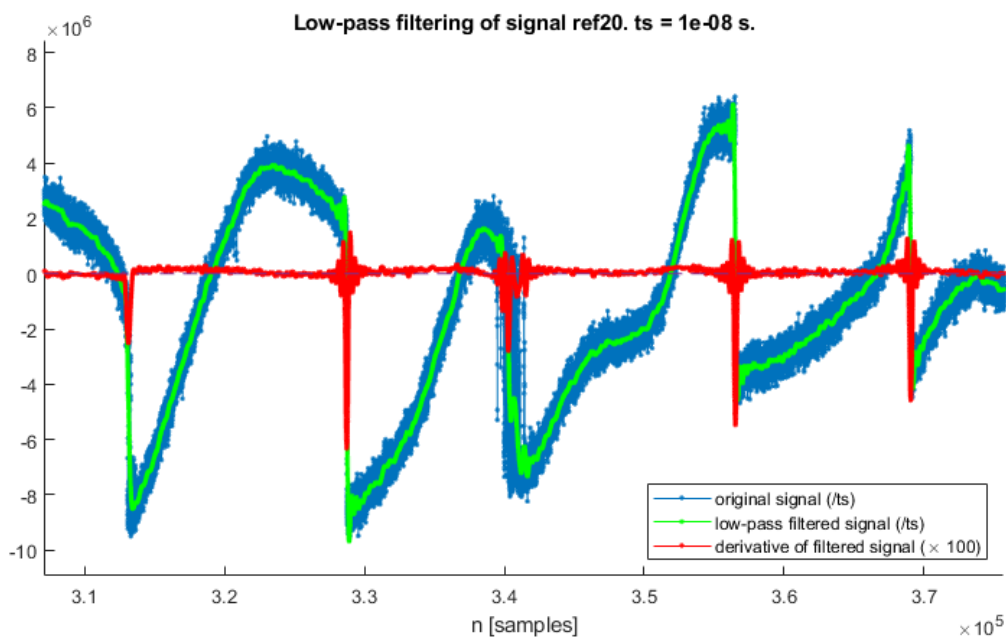
Figure 28 : Derivative of filtered signal for a slow fringe with oscillations

Figure 28 shows some slow fringes before and after filtering, including the one in Figure 27. As can be seen, for fringes 2, 4, and 5 from left to right, the derivative clearly identifies the jump in the fringe. For fringes 1 and 3, the peaks in the derivative are not very noticeable and

this is due to the oscillations present in these fringes. For fringe 3, for instance, the derivative presents various peaks, which mark the oscillations still present in the filtered signal in Figure 27. With regards to the noise present in the derivative, it is visually lower compared to the noise present in the derivative of the unfiltered signal. Figure 29 shows more fringes and the peaks in the derivative showing the jump discontinuities in the fringes, it is also seen that in this case, the peaks in the derivative are very clearly defined, and the low noise visible aids in spotting the peaks more clearly.
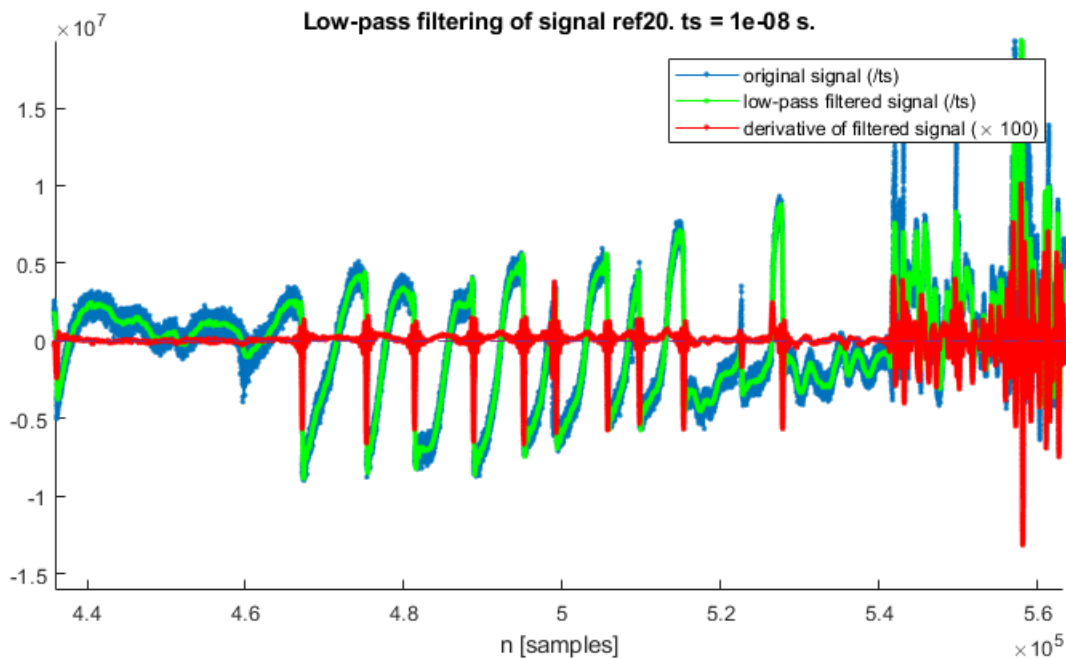
Figure 29 : SM signal ref20, filtered signal and derivative of filtered signal

The application of the LP filter, however, is not a perfect solution to identify the slow-oscillating fringes. This is shown by Figure 30, which shows other region of slow fringes in the ref20 signal, that have a higher frequency but not so that they can be considered fast fringes. In this case, the filtered signal is shown not to keep the shapes of some fringes found in the unfiltered signal: for instance, the two fringes encircled on the left are not distinguishable after filtering. As a consequence, when deriving the filtered signal, the peaks in the derivative are

not large enough to be used for fringe identification. On the fringe encircled on the right, it can be seen that the jump discontinuity is not well captured in the filtered signal since this last doesn't have a jump anymore. This causes the derivative to not have a peak as high as it would have had if the jump discontinuity had been captured in the filtered signal. In conclusion, it is not possible to detect all slow fringes with the current LP filter.
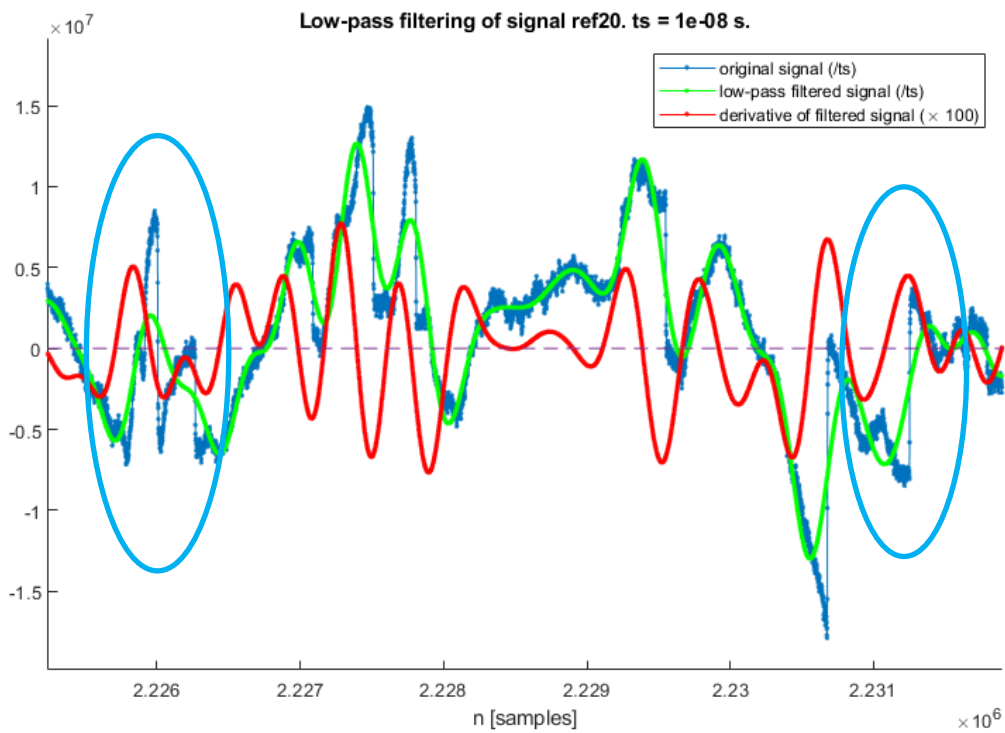
Figure 30 : Filtered signal does not always provide a good representation of the fringes

CONCLUSIONS

It can be concluded that the analysis of region 1 from 2 different signals to compare the MW and D algorithms was not enough and more of these regions should be analyzed. The important variable that may be influencing the conclusion as to which algorithm is better is the thresholding, which is done by hand. So, to remove the effect of the thresholding on the conclusion, many of these fast regions should be analyzed. It was seen, however, that the fringe directions are better detected using the D algorithm, and this is thanks to the derivative that doesn't have a shift as opposed to the original derivative used in Maiwenn's algorithm.

With regards to the automatic detection of the fast regions, it was not possible to do it by using the CWT, and this is because the fast frequency components of the slow fringes get confused with the fast fringes when plotting the spectrogram.

With regards to the low-pass filter designed, it was found that it does not always detect well the slow fringes, because sometimes the filtering distorts the fringes, making the detection of their jump discontinuities by using the derivative impossible.

REFERENCES

Bernal, O., Seat, H., Zabit, U., Surre, F., & Bosch, T. (2015). Robust Fringe Detection Based on Bi-Wavelet Transform for Self-Mixing Displacement Sensor. *IEEE*.

Berthelot, M. (2020). *Etude de la propagation d'ondes de choc par interrogation optique avec un capteur laser par réinjection optique.*

Bertling, K., Perchoux, J., Taimre, T., Malkin, R., Robert, D., Rakic, A., & Bosch, T. (2014). Imaging of acoustic fields using optical feedback interferometry. *Optical Society of America*.

Imas, J. J. (2019). *Optical Feedback Interferometry for pressure measurement in detonics.*

Sauer, T. (2012). *Numerical Analysis.* Pearson.

Taimre, T., Nikolic, M., Bertling, K., Leng Lim, Y., Bosch, T., & Rakic, A. (2015). Laser feedback interferometry: a tutorial on the self-mixing effect for coherent sensing. *Advances in Optics and Photonics*, 570-631.
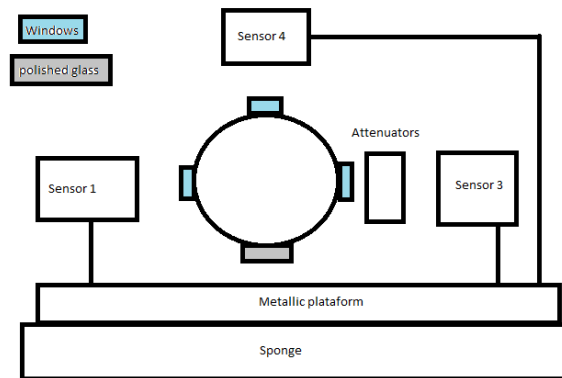
INDEX OF ANNEXES

ANNEX A: ANNOTATIONS OF THE CEA EXPERIMENTS PERFORMED ON JULY 1ST, 2021

Experiments with windows

Set up.

Figure 31: Sensors at the end of shock tube

Conditions common to all experiments.

The following conditions were the same for all 3 experiments, except where indicated.

Laser conditions

Laser collimated for all 3 sensors

Sensor 4: no attenuator; sensors 1 and 3: attenuators different for each experiment

	Sensor 1	Sensor 3	Sensor 4
Beam	Collimated	Collimated	Collimated
Lens	C230TME-C	C240TME-C	C660TME-C
Target surface	Metallic surface of sensor 3	Green PCB surface of sensor 1	Polished glass in shock tube
Distance from laser's lens to target [cm]	24.9	26.68	22.4

Acquisition system connections.

Sensor 1	Channel 1
Sensor 3	Channel 2
Sensor 4	Channel 3

Oscilloscope connections.

Except for experiment 1, where the oscilloscope wasn't used:

Sensor 1	Channel 1
Sensor 3	Channel 3
Sensor 4	Channel 4

Measurements.

Experiment 1

Pressure change : 1 –> 5 bar

Attenuators :

Sensor 1	Attenuator 3 from bottom
Sensor 3	Attenuator 5 from bottom

Experiment 2

Pressure change : 1 -> 5 bar

Attenuators :

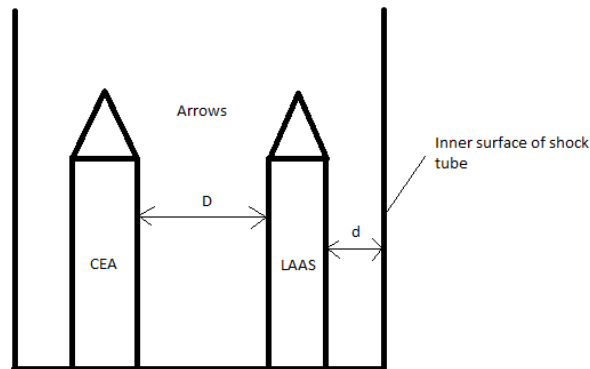| Sensor 1	Attenuator 4 from bottom
Sensor 3	Attenuator 6 from bottom

Experiment 3

Pressure change : 1 -> 15 bar

Attenuation : Same as in experiment 2

Observation: Maylin's reference sensor got saturated. It was not fit for 15 bar.

Experiments with arrow

Set up.

D: distance from laser's lens to CEA arrow's surface. D = 3 - 3.5 cm
d: distance from laser's lens to inner surface of shock tube. d = 2.5 cm

Figure 32 : Arrow experiment set-up

Conditions common to all experiments.

- Laser: collimated

The CEA's arrow has 2 pressure sensors, a front one and a rear one. In all experiments, our laser was closer to the rear sensor.

Measurements.

Experiment 1

Pressure change: 1 -> 5 bar

Laser's target: inner surface of shock tube

Experiment 2

Same conditions as experiment 1

Experiment 3

Pressure change: 1 –> 15 bar

Laser's target: inner surface of shock tube

Experiment 4

Pressure change: 1 -> 5 bar

Laser's target: CEA arrow's surface.